

RAPID TEV VARIABILITY IN BLAZARS AS RESULT OF JET-STAR INTERACTION

M.V. BARKOV^{1,2}, F.A. AHARONIAN^{3,1}, S.V. BOGOVALOV⁴, S.R. KELNER^{1,4}, AND D. KHANGULYAN⁵

¹Max-Planck-Institut für Kernphysik, Saupfercheckweg 1, D-6917 Heidelberg, Germany; bmv@mpi-hd.mpg.de

²Space Research Institute RAS, 84/32 Profsoyuznaya Street, Moscow, 117997, Russia

³Dublin Institute for Advanced Studies, 31 Fitzwilliam Place, Dublin 2, Ireland

⁴National Research Nuclear University (MEPHI), Kashirskoe shosse 31, 115409 Moscow, Russia and

⁵Institute of Space and Astronautical Science/JAXA, 3-1-1 Yoshinodai, Chuo-ku, Sagamihara, Kanagawa 252-5210, Japan

Draft version October 27, 2018

ABSTRACT

We propose a new model for the description of ultra-short flares from TeV blazars by compact magnetized condensations (blobs), produced when red giant stars cross the jet close to the central black hole. Our study includes a simple dynamical model for the evolution of the envelope lost by the star in the jet, and its high energy nonthermal emission through different leptonic and hadronic radiation mechanisms. We show that the fragmented envelope of the star can be accelerated to Lorentz factors up to 100 and radiate effectively the available energy in gamma-rays predominantly through proton synchrotron radiation or external inverse Compton scattering of electrons. The model can readily explain the minute-scale TeV flares on top of longer (typical time-scales of days) gamma-ray variability as observed from the blazar PKS 2155–304. In the framework of the proposed scenario, the key parameters of the source are robustly constrained. In the case of proton synchrotron origin of the emission a mass of the central black hole of $M_{\text{BH}} \approx 10^8 M_{\odot}$, a total jet power of $L_j \approx 2 \times 10^{47} \text{ erg s}^{-1}$ and a Doppler factor, of the gamma-ray emitting blobs, of $\delta \geq 40$ are required. Whilst for the external inverse Compton model, parameters of $M_{\text{BH}} \approx 10^8 M_{\odot}$, $L_j \approx 10^{46} \text{ erg s}^{-1}$ and the $\delta \geq 150$ are required.

Subject headings: galaxies: jets — Gamma rays: galaxies — BL Lacertae objects: individual (PKS 2155–304)

1. INTRODUCTION

The flux variability of very high energy (VHE) gamma-rays on minute timescales detected from the BL Lac object PKS 2155–304 (Aharonian et al. 2007) and Mkr 501 (Albert et al. 2007) challenges the standard scenarios suggested for the explanation of the nonthermal properties of TeV blazars (Begelman et al. 2008; Giannios et al. 2009). The extremely short duration of the flares impose severe constraints on the size of the gamma-ray producing region, of

$$l' \leq c\tau' \simeq 3 \times 10^{13} \tau_3' \text{ cm}, \quad (1)$$

where l' and $\tau_3' = \tau'/10^3 \text{ s}$ are the proper production size and the variability timescale in the frame of the jet respectively and c is the light speed. The proper variability time-scale, τ' , is connected to the variability in the observer frame, τ , by the relation

$$\tau = \frac{\tau'}{\delta}, \quad (2)$$

where δ is the Doppler factor of the moving source (the blob):

$$\delta = \frac{1}{\Gamma(1 - \beta \cos(\alpha))}. \quad (3)$$

Here the bulk Lorentz factor, Γ , accounts for the relativistic transformation of time, and $(1 - \beta \cos(\alpha))$ is responsible for the kinematic shrinking of the duration of the radiation and $\beta = v/c$.

Relativistic jets ejected from the central engines are common phenomena for different types of active galactic nuclei (AGN). In particular, apparent superluminal

speeds $\beta_{\text{app}} = \beta \sin \alpha / (1 - \beta \cos \alpha)$ (in units of the speed of light c) as high as ~ 40 have been detected for radio components on (projected) scales of $\sim 1 - 10 \text{ pc}$ (see e.g. Jorstad et al. 2001, 2005; Marscher et al. 2010) in blazars - AGN with jets directed to the observer. This implies very large Lorentz factors of bulk motion given that $\Gamma \geq \beta_{\text{app}}$.

Because of the large bulk Lorentz factors of TeV blazars, the condition Equation (2) allows significant relaxation of the requirement supplied by Equation (1). In particular, Levinson & Bromberg (2008) argued that if a perturbation is produced by the central engine, its size should exceed the gravitational radius of the black hole in the observer frame. Consequently, the proper size of the production region is expected to be larger than Γr_g , where $r_g = GM_{\text{BH}}/c^2 \approx 1.5 \times 10^{13} M_{\text{BH},8} \text{ cm}$ is the gravitational radius of a black hole (BH) of mass $M_{\text{BH},8} = M_{\text{BH}}/10^8 M_{\odot}$. In this case, the variability time-scale $\tau_2 = \tau/10^2 \text{ s}$ imposes a strict upper limit on the gravitational radius:

$$r_g < 3 \times 10^{12} \tau_2 \frac{\delta}{\Gamma} \text{ cm}. \quad (4)$$

Thus, the detection of gamma-ray flux variability $\tau \sim 200 \text{ s}$ constrains the BH mass, to be $M_{\text{BH},8} < 1$. In reality, since the main energy release occurs in the inner parts of the accretion disk of radius $r \sim 10 r_g$, the mass of the black hole should be close to $10^7 M_{\odot}$. Generally, in the case of an extreme Kerr black hole, the energy release takes place at the gravitational radius. However, even in this case one needs an entire rotation period for an effective energy release, i.e. the characteristic time cannot be much shorter than $2\pi r_g/c$. This implies that

even in this case the upper bound of the BH mass of $10^7 M_\odot$ cannot be significantly relaxed.

This conclusion is true, in particular, for the model of internal shocks. Note, however, that it is based on the assumption that the perturbation (the reason of the flare) originates in the central engine. Therefore it cannot be unconditionally extended to other possible scenarios as is claimed by Dermer et al. (2009). Indeed, Equation (4) is not valid if perturbations are produced by an external source, e.g. by plasma condensations (often called "blobs") which do not have a direct link to the central black hole. Such blobs can be produced, in particular, by interactions of stars with the base of the jet, as proposed by Barkov et al. (2010) to explain the TeV flares of M 87 on scales of days (see also Araudo et al. 2010), where the interaction of gas clouds from broad line regions are discussed). The jet power of M 87 is relatively modest, $L_j \simeq 10^{44} \text{ erg s}^{-1}$. The results of Barkov et al. (2010) show that, while this power is sufficient to blow-up the envelope (atmosphere) of the star which initially has been pulled out by the tidal force of the BH, such a jet appears to be not sufficiently powerful for acceleration of the gas cloud to relativistic velocities. Actually this works in a positive direction for M 87, given the large aspect angle of the jet. Otherwise, the gamma-ray flux could not be observed because of the Doppler de-boosting effect. On the other hand, the suggested mechanism of formation of hadronic blobs in the jets cannot apply to powerful gamma-ray blazars unless the blobs are accelerated to Lorentz factors $\Gamma \geq 10$. Remarkably, this can be realized in a quite natural way in powerful jets with $L_j \geq 10^{46} \text{ erg s}^{-1}$. Interestingly, such powerful jets can ablate the star atmosphere without help of tidal forces (the interesting implications of this effect are discussed below). Moreover, the powerful jets can drag and disrupt the star's envelope into an ensemble of blobs moving with large Lorentz factors which, from the point of view of explanation of very short time variability is a quite comfortable situation.

Another important aspect of the short time variability is related to the efficiency of acceleration and radiation mechanisms. Currently the most conventional approach for modeling of VHE emission production in active galaxies is based on the inverse Compton (IC) scattering of relativistic electrons, the soft target photon field being either the synchrotron radiation of same electrons (the so-called Synchrotron-self Compton (SSC) model), or provided by external sources (EIC model). The apparent advantage of IC models is the combination of two factors: (1) the acceleration of electrons to relatively modest energies ($\leq 1 \text{ TeV}$) can be effectively realized within different acceleration scenarios; and (2) these electrons radiate readily in interactions of ambient radiation and magnetic fields. Nevertheless, while the IC models allow rather satisfactory explanations of the energy spectra and variability patterns of many blazars in general, the parameters used to fit some specific objects appear incompatible with the parameters defined from observations. Moreover, the observed short variability time-scale demands conditions which appear to be quite uncomfortable, in terms of the strength of magnetic field and related consequences concerning the strong deviation from equipartition between the energy density of rela-

tivistic electrons and magnetic fields. The requirement of weak, (generally less than 1 G) magnetic fields is one of the key postulates of the IC paradigm of gamma-ray production in blazars. Moreover, in the case of some objects with unusually hard source spectra (after correction for intergalactic absorption), such as 1ES 0229+200, the magnetic field is required to be as small as 1mG (Tavecchio et al. 2009). The magnetic field in the blazar jets can be reduced to such small values only at very large distances from the central engine, namely $\gtrsim 10^{18} \text{ cm}$. Although this idea has some observational support related to the transparency of blobs in the radio band (Marscher et al. 2008), it is likely that regions of highly variable gamma-ray emission are located at smaller distances from the central engine (Tavecchio et al. 2010). In particular, the EIC models require the location of any gamma-ray emitter to be located closer to the BH into the so-called Broad Line Regions (BLR), i.e typically at distances $R \sim 10^{17} - 10^{18} \text{ cm}$. This implies that any IC model can be realized only if one finds a way dramatically reduce the magnetic field in the jet. Although this cannot be excluded (e.g. because of reconnection of the B-field (Komissarov et al. 2007a; Giannios et al. 2009; McKinney & Uzdensky 2010) or due to the effective bulk acceleration of plasma (Komissarov et al. 2010; Tchekhovskoy et al. 2010)), strong magnetic fields exceeding 1 G remain a more favored option, as long as we deal with strong jets on sub-parsec scales. In this regard, the models which invoke high energy protons for the production of gamma-rays passes certain advantages despite a quite popular view that they are not effective emitters (see e.g. Sikora 2010). Actually this is true only for proton-proton and proton-photon interactions. What concerns the synchrotron radiation of protons, with a key assumption on the acceleration of particles with a rate close to $t^{-1} \sim ceB/E$, where E is the proton energy, coupled with a strong magnetic field between 10 to 100 Gauss, and a large Doppler factor, $\delta \geq 10$, it is that can provide relevant acceleration and radiation timescales, as well as explain the extension of gamma-ray spectra to TeV energies (see e.g. Aharonian 2000).

2. BLOBS IN RELATIVISTIC JETS

2.1. AGN Jet – Red Giant interaction

Below we discuss the distinct features of the interaction of red giants with AGN jets in the specific case of powerful blazars, see sketch of the scenario in Figure 1. Originally, the scenario of AGN jet – red giant (RG) interaction has been suggested by Barkov et al. (2010) for the explanation of VHE observations of M87 - a non-blazar type nearby AGN with a large jet viewing angle of $\geq 20^\circ$ and a modest jet power, of $L_{\text{jet}} \simeq 10^{44} \text{ erg s}^{-1}$. It was demonstrated that if disturbed by tidal forces RG penetrates the jet, the ram pressure of the jet in M87 would be sufficient to remove the outer layer of the RG. This leads to the formation of a dense cloud within the jet which, in combination with effective particle acceleration, can trigger gamma-ray production through proton-proton interactions which passes secure of the required spectral and temporal properties. This model allows detectable gamma-ray fluxes because of the proximity of the source and the non-relativistic speed of the blobs (otherwise the radiation from M87 would be de-boosted

given the large aspect angle of the jet).

The AGN jet – red giant interaction (JRGI) has very specific and important features in the case of powerful blazars, where the ram pressure can be as high as

$$P_{\text{ram}} \simeq 10^3 L_{j,46} z_{17}^{-2} \theta_{-1}^{-2} \text{ dyn cm}^{-2}. \quad (5)$$

Here $L_{j,46} = L_j/10^{46} \text{ erg s}^{-1}$, $z_{17} = z/10^{17} \text{ cm}$ and $\theta_{-1} = \theta/0.1$ are the jet power, the distance from the BH, and the jet opening angle, respectively. Such a high ram pressure can blow-up the outer layers of the stellar atmosphere, even from a non-disturbed RG. The mass of the removed layer can be roughly estimated from the balance of the jet ram force to the gravitational force, $P_{\text{ram}} \pi R_*^2 \simeq G \Delta M M_* / R_*^2$. Here M_* and R_* are the RG mass and radius, respectively. This gives the mass of the cloud stripped from the star by the jet:

$$\Delta M = \frac{\pi P_{\text{ram}} R_*^4}{G M_*} \approx 6 \times 10^{28} L_{j,46} z_{17}^{-2} \theta_{-1}^{-2} R_{*,2}^4 M_{*,0}^{-1} \text{ g}, \quad (6)$$

where $R_{*,2} = R_*/10^2 R_\odot$ and $M_{*,0} = M_*/M_\odot$ are the RG parameters expressed through the solar mass (M_\odot) and radius (R_\odot). This estimate illustrates the feasibility of formation of a cloud due to the JRGI process. The next important issue is the acceleration of the cloud in the jet. In what follows, we assume that initially the ejected matter from the RG envelope forms a (quasi) spherical cloud of radius comparable to the RG size, $r_c \simeq R_*$.

To be accelerated, the matter residing in the jet first should be heated, thus the cloud expands enhancing the interaction between the cloud and the jet. A significant expansion occurs on a time-scale of $t_{\text{exp}} = A t_{\text{cc}}$, where A is a constant of order of 5 (see e.g. Gregori et al. 2000; Nakamura et al. 2006; Pittard et al. 2010), and $t_{\text{cc}} = 2r_c/c_s$ is the sound crossing time. Here c_s is the sound speed in the shocked cloud, which can be estimated as $c_s^2 \approx \gamma_g P_{\text{ram}}/\rho_c \approx \gamma_g P_{\text{ram}} 4\pi r_c^3/(3M_c)$ ($\gamma_g = 4/3$ is the plasma adiabatic coefficient). This gives the following estimate for the expansion time:

$$t_{\text{exp}} = A t_{\text{cc}} = 5 \times 10^5 R_{*,2}^{-1/2} M_{c,26}^{1/2} L_{j,46}^{-1/2} z_{17} \theta_{-1} \text{ s}, \quad (7)$$

where $M_{c,26} = M_c/10^{26} \text{ g}$ is the normalized mass of the cloud. The orbital velocity of a star around the black hole,

$$V_{\text{orb}} \approx \sqrt{\frac{GM_{\text{BH}}}{z}} \approx 4 \times 10^8 M_{\text{BH},8}^{1/2} z_{17}^{-1/2} \text{ cm s}^{-1}, \quad (8)$$

results in a crossing time of the jet of

$$t_{\text{jc}} \approx \frac{z^{3/2} \theta}{\sqrt{GM_{\text{BH}}}} = 3 \times 10^7 z_{17}^{3/2} \theta_{-1} M_{\text{BH},8}^{-1/2} \text{ s}. \quad (9)$$

The condition $t_{\text{exp}} < t_{\text{jc}}$ defines an upper limit on the mass of the cloud, which can expand in the jet:

$$M_{c,sc} \lesssim 3 \times 10^{29} L_{j,46} R_{*,2} z_{17} M_{\text{BH},8}^{-1} \text{ g}. \quad (10)$$

If this constraint is fulfilled, then at the stage of hydrodynamical expansion, the cloud can increase its linear size by a few orders of magnitude (see e.g. Pittard et al. 2010) whilst remaining in the jet.

The cloud will be trapped by the jet if it would be sufficiently accelerated along the jet axis. Thus, the confinement condition has the following form: $v_z = a_z t_{\text{jc}} >$

V_{orb}/θ , where $a_z = P_{\text{ram}} \pi r_c^2/M_c$. Using Equations (5) and (9) one obtains the cloud capture condition:

$$M_{c,jc} \lesssim 3 \times 10^{31} L_{j,46} r_{c,15}^2 M_{\text{BH},8}^{-1} \text{ g}, \quad (11)$$

where $r_{c,15} = r_c/10^{15} \text{ cm}$ is the size of the cloud after the hydrodynamical expansion. Importantly, Equations (10) and (11) provide upper limits, which exceed significantly the expected mass of the blown-up layer given by Equation (6). Thus, even if the ablated stellar matter remains as one blob, this cloud will still be trapped in the jet and accelerated up to sub-relativistic velocities (i.e. $\sim 0.1c$). In fact, independent of the initial conditions, during the acceleration phase the cloud is expected to be crushed into hundreds of small blobs (Pittard et al. 2010). This relaxes significantly the above obtained conditions, since the ensemble of blobs can be more easily picked up by the jet flow.

2.2. Relativistic Stage

At the relativistic stage, the dynamics of the cloud is described by the following equation:

$$\frac{d\Gamma_c}{dt} = \left(\frac{1}{\Gamma_c^2} - \frac{\Gamma_c^2}{\Gamma_j^4} \right) \frac{L_j r_c^2}{4\omega^2 c^2 M_c}, \quad (12)$$

where Γ_c is the Lorentz factor of the cloud, $\omega \approx z\theta$ is cylindrical radius of the jet (see Appendix A for the derivation of Equation (12)). Let us introduce the following notations $g \equiv \Gamma_c/\Gamma_j$ and $y \equiv z/z_0$ (and $dy \approx c dt/z_0$). Here z_0 is the distance from the BH to the point where the RG penetrates the jet, i.e., we adopt the initial condition $g \ll 1$ at $z = z_0$. Several simplifications, in particular, assuming that $\Gamma_j = \text{const}$ on the cloud acceleration time scale, and $dt = dy z_0/c$, allow presentation of Equation (12) in the form:

$$\frac{dg}{dy} = \left(\frac{1}{g^2} - g^2 \right) \frac{D}{y^2}, \quad (13)$$

where

$$D \equiv \frac{L_j r_c^2}{4\theta^2 \Gamma_j^3 z_0 c^3 M_c}. \quad (14)$$

Equation (13) allows an analytical solution, which defines y as a function of g and D .

In this paper we do not specify the origin of relativistic particles in the cloud. However, assuming that particle acceleration is a result of a strong interaction between the cloud and the jet, we may conclude that high Lorentz factors do not support the production of non-thermal radiation. Indeed, as it follows from Equation (13), the cloud-jet interaction intensity decreases with cloud acceleration. The apparent intensity of the non-thermal phenomena can be roughly described by the luminosity correction function F_e , which accounts both for the Doppler boosting, i.e. $F_e \propto \Gamma_c^4$, and for the interaction intensity, i.e. $F_e \propto \left(\frac{1}{\Gamma_c^2} - \frac{\Gamma_c^2}{\Gamma_j^4} \right) / z^2$. For the sake of clarity, we consider the correction function in dimensionless form $F_e = g^4 (1/g^2 - g^2) / y^2$. Since the solution of Equation (13) relates g and y , F_e is, in fact, a function of one variable. In Figure 2, we show it as a function of g (left panel) and as a function of the variable $\varkappa = t(1 - V_c)/t_0 = 2D(y - 1)\Gamma_j^2(1 - V_c)$ (right

panel), corresponding roughly to the observation time (here $V_c = \sqrt{1 - \Gamma_c^{-2}}$ is the blob velocity). The values of the parameter $D = 0.1, 1, 10$ and 100 are used in both panels of Figure 2. It can be seen that in the case of $D \gtrsim 1$, the solution depends weakly on the parameter D , and the non-thermal activity of the blob is expected to have a narrow peak of duration:

$$t_0 \approx \frac{z_0}{c} \frac{1}{D} \frac{1}{2\Gamma_j^2}. \quad (15)$$

The maximum of the correction function occurs at $g_{\max} \approx 0.8$.

In the case of $D \ll 1$, the situation is quite different. Namely, the expected nonthermal activity has no pronounced peak, thus such a blob cannot produce a high-amplitude flare. In this regard, we can formulate the condition $D \gtrsim 1$ as a requirement for a flaring episode. This condition can be reformulated as an upper limit on the cloud mass:

$$M_{c,rc} \lesssim \frac{L_j r_c^2}{4\theta^2 c^3 z \Gamma_j^3}. \quad (16)$$

The above relation depends not only on the properties of the cloud (its size and mass) but also on the jet power and Lorentz factor. Thus, for quantitative calculations, one needs detailed information about the dynamics and properties of the blazar jet.

Although the process of jet formation is not fully understood, recent hydrodynamical studies of different scientific groups show that the Blandford-Znajek (Ruffini & Wilson 1975; Lovelace 1976; Blandford & Znajek 1977) process may be at work in AGN, and suggest a concept of magnetically accelerated jets. Thus, the jet base is expected to be strongly magnetized and likely magnetically dominated at $z \leq 1$ pc (Komissarov et al. 2007b; Barkov & Komissarov 2008; Beskin 2010). This immediately gives the magnetic field strength of the jet in laboratory frame

$$B_j \approx \left(\frac{4L_j}{cz^2\theta^2} \right)^{1/2} \approx 120 L_{j,46}^{1/2} z_{17}^{-1} \theta_{-1}^{-1} \text{ G}. \quad (17)$$

During the jet propagation, the magnetic field energy can be transformed to the bulk kinetic energy. At the linear stage a simple relation defines the bulk Lorentz factor (Beskin & Nokhrina 2006)

$$\Gamma_j \approx \frac{\omega}{4r_g}. \quad (18)$$

Finally, the opening angle of the jet is expected to be $\theta \approx 1/\Gamma_j$ (Komissarov et al. 2009). Combining Equations (17) and (18), one can estimate the magnetic field in the jet comoving frame,

$$B_c \approx \frac{2}{z} \left(\frac{L_j}{c} \right)^{1/2} \approx 12 z_{17}^{-1} L_{j,46}^{1/2} \text{ G}. \quad (19)$$

In Figure 3, the typical magnetic field and bulk Lorentz factors of the jet are shown for three different distances from the BH. These values are in good agreement with observed values of magnetic field on parsec scales in AGNs (Lobanov 1998; Savolainen et al. 2008; O’Sullivan & Gabuzda 2009; Sokolovsky et al. 2010).

Using Equation (18), one can present Equation (16) in the form

$$M_{c,rc} \lesssim 0.5 \times 10^{26} L_{j,46} r_{c,15}^2 \Gamma_{j,1.5}^{-3} M_{\text{BH},8}^{-1} \text{ g}. \quad (20)$$

Note that at this late stage, the cloud can be already significantly expanded with a radius of $r_{c,15} \gg 1$. The extreme value of $M_{c,rc}$ can be achieved at $r_c \approx \omega$:

$$M_{c,rc} \lesssim 2 \times 10^{26} L_{j,46} M_{\text{BH},8} \Gamma_{j,1.5}^{-1} \text{ g}. \quad (21)$$

This upper limit is more robust than the constraints given by Equations (6),(10), and (11), we note however, that it concerns the mass of the blob, but not the mass of the ablated stellar atmosphere.

2.3. Energy Budget of the Cloud

Below we consider the general requirements to the scenario in the context of blob’s radiation efficiency. These constraints have a quite basic character and are not related to a specific radiation mechanism. Obviously, the gamma-ray production mechanisms impose additional requirements, concerning e.g. the density of relevant targets in the form of gas, radiation or magnetic field. We discuss the impact of specific radiation mechanisms in Section 3. Here we try to find a generic link between properties of a blob, which is responsible for the non-thermal emission, to the parameters of the AGN, i.e. the mass of the central engine and the jet power.

Emission detected from blazars are significantly enhanced due to Doppler boosting. The apparent (L_γ) and intrinsic (L_{sc}) luminosities are connected through the well known relation: $L_\gamma = L_{sc} \delta_c^4$ (here δ_c is Doppler factor of the production region). On the other hand, the intrinsic luminosity of the blob can be expressed as a fraction ξ of the power transferred by the jet to the blob:

$$L_{sc} = \xi \left(\frac{1}{\Gamma_c^2} - \frac{\Gamma_c^2}{\Gamma_j^4} \right) \frac{L_j r_c^2}{4\omega^2}. \quad (22)$$

The parameter $\xi \ll 1$ accounts for the overall efficiency of transformation of the absorbed jet energy to non-thermal emission through acceleration and radiation of relativistic particles (note that the righthand-side of the Equation (22) refers to the quantities in the observer frame, whilst the lefthand-side corresponds to the blob’s reference frame). For small aspect angles, $\delta \approx 2\Gamma_c$, we thus obtain the following simple relation:

$$L_\gamma = 4\xi F_e L_j \Gamma_j^2 \frac{r_c^2}{\omega^2}, \quad (23)$$

which has a few interesting implications. In particular, one can estimate the size of the blob:

$$r_c = \frac{\omega}{\Gamma_j} \left(\frac{L_\gamma}{4\xi F_e L_j} \right)^{1/2}. \quad (24)$$

Given the standard bulk Lorentz factors, $\Gamma_j \approx \omega/(4r_g)$, and the maximum of correction function, $\max(F_e) \approx 0.4$, together with conventional normalizations, one obtains

$$r_c \approx 5 \times 10^{14} M_{\text{BH},8} L_{\gamma,47}^{1/2} L_{j,46}^{-1/2} \xi_{-1}^{-1/2} \text{ cm}. \quad (25)$$

Here we use quite a high normalization for the efficiency, of $\xi_{-1} = \xi/0.1$

Another important estimate can be obtained for the maximum apparent luminosity of the blob. It is achieved when the blob eclipses the whole jet, i.e. $r_c \approx \omega$. In this case, one obtains:

$$L_{\gamma \max} = 2 \times 10^{48} \xi_{-1} L_{j,46} \Gamma_{j,1.5}^2 \text{ erg s}^{-1}. \quad (26)$$

where $\Gamma_{j,1.5} = \Gamma_j/10^{1.5}$. Note that the apparent non-thermal luminosity of the blob is proportional to Γ_j^2 . Remarkably, even for relatively modest values of the jet Lorentz factor, $\Gamma_j \sim 10$, and the conversion efficiency, $\xi \sim 0.01$, L_γ is comparable to the jet power.

2.4. Time variability

The fast variability of TeV gamma-ray emission of blazars, which can be as short as a few minutes as reported for PKS 2155–304 (Aharonian et al. 2007) and Mkr 501 (Albert et al. 2007), is a key observational fact which should be addressed by any model of TeV blazars. In addition to a general (standard) statement about the strongly *Doppler boosted* gamma-ray emission produced in very *compact regions* close to the central black hole, any dedicated model should provide intrinsic reasons for variability (characterizing the scenario as a whole) and offer radiation mechanisms with adequate cooling times. If the cooling time-scale appears to be too long, an alternative source of the variability is required. For example, a change of the production site velocity may lead to a strong change in the apparent luminosity. Indeed, since the production region is to be Doppler boosted, a variation of the Doppler factor may be a plausible reason for strong variation of the observed flux.

In this section, we discuss the variability scales related to this effect, and its implication to the JRGI scenario. We note that the relevant time-scales do not depend on the cooling time of the emitting particles. In particular, the obtained size of the blob in Equation (25) and the jet Lorentz factor provide following lower limit on the variability time-scale:

$$\tau > \frac{r_c}{\Gamma_j c} \approx 4 \times 10^2 z_{17}^{-1/2} L_{\gamma,47}^{1/2} L_{j,46}^{-1/2} \xi_{-1}^{-1/2} M_{\text{BH},8}^{3/2} \text{ s}, \quad (27)$$

which appears to be close to the observed one, and can be significantly shorter in the case of powerful jets.

2.4.1. Duration of the blob-jet interaction

The principal variability scale in the JRGI scenario is related to the duration of the effective interaction of the cloud with the jet and is determined by the function F_e (see Section 2.2). Since the model requires very effective acceleration of particles, with a $\geq 10\%$ efficiency of the energy transformation to nonthermal particles, the shape of the function, F_e , (see Figure 2) can be treated as the time profile of particle acceleration with a characteristic timescale:

$$\Delta t \approx \frac{2z_0^2 \theta^2}{r_c^2} \frac{\Gamma_j c^2 M_c}{L_j}. \quad (28)$$

Note that in the extreme case, when the blob eclipses the entire jet, i.e. $z_0^2 \theta^2 / r_c^2 \sim 1$, the characteristic time-scale, Δt , depends only on the jet Lorentz factor Γ_j and power L_j , as well as on the mass of the cloud M_c :

$$\Delta t \approx 60 \Gamma_{j,1.5} L_{j,46}^{-1} M_{c,25} \text{ s}, \quad (29)$$

The total apparent energy of electromagnetic radiation which can be emitted by the cloud can be estimated from Equations (26) and (29):

$$E_{\text{tot}} \approx 10^{50} \xi_{-1} M_{c,25} \Gamma_{j,1.5}^3 \text{ erg}. \quad (30)$$

For the values expected in this scenario (which were also used for normalization of Γ_j , L_j and M_c in Equation (29)), the cloud-jet interaction can be quite brief; - shorter than the detected variability of the ultrafast flares of PKS 2155–304 and Mkn 501. Moreover, for small mass clouds, it can be as short as 1 sec. Obviously, this time-scale corresponds to the flare rising interval, while fast emission decay requires short radiative or adiabatic cooling of the emitting particles or rapid changes in the blob's Doppler factor.

2.4.2. Helical structure of relativistic jet

Generally, in powerful jets, the change of the Doppler factor is unavoidable. Indeed, since the matter in the jet moves along the dominant magnetic field lines, which are expected to be helical, the velocity of the blob should have both poloidal and azimuthal components. The azimuthal velocity can be as high as $v_\phi \approx cr_{lc}/\omega$ (Beskin & Nokhrina 2006; Komissarov et al. 2007b; Beskin 2010), where $r_{lc} \sim 4r_g$ is light cylinder radius, therefore, during the motion, the angle towards the direction to observer can be changed. We discuss the corresponding variability pattern in Appendix B, where it is shown that this effect (which reminiscent to some extent, the operation of a 'revolver'), can lead to a change in the flux by a factor of 2 if the blob has $v_\phi \sim 0.5c$ and turns around the jet axis by an angle of $\sim \pi/4$. In the case of magnetically driven jet using Equation (18) we can get $v_\phi \approx c/\Gamma_j$ or if $\Gamma_j > 3$ this mechanism cannot to explain variability of blazars.

2.4.3. Collision of blobs

The interaction of the jet with a massive cloud leads unavoidably to the formation of a large number of small blobs, which may gain an additional chaotic velocity component. Let us assume that the chaotic velocity is comparable to the sound speed in relativistic gas, i.e. $v_s \sim c/\sqrt{3}$, which is larger than $c/2$, that is enough to explain strong radiation variability (see for details Appendix B). Due to interactions with each other, the blobs can change their speeds on timescales $t_s \sim 2r_c/v_s$ leading to the variability on a timescale

$$\tau \approx t_s / \delta \gtrsim 5 \times 10^2 M_{\text{BH},8} L_{\gamma,47}^{1/2} L_{j,46}^{-1/2} \xi_{-1}^{-1/2} \delta_2^{-1} \text{ s}, \quad (31)$$

where Doppler factor is determined as $\delta_2 = \delta/10^2$.

Equation (29) shows that the interaction time-scale in the JRGI scenario could be very short allowing, in the case of comparably short particle cooling time, flaring episodes of duration ~ 100 s. If the particle cooling mechanism cannot provide the required energy loss rate, the nonthermal flux variability can be caused by a change in the production region Lorentz factor, see e.g. Equation (31). However, we note that in this case the variability on timescales as short as 100 s would require a rather specific combination of several principal parameters. Thus, a radiative mechanism with short cooling

time remains still a quite feasible requirement for models intended to explain the fast variability observed in blazars.

In the following section we discuss the efficiency and features of major radiation mechanisms related to both protons and electrons. Although the jet composition is still debated, the conventional approach attributes the non-thermal activity of AGN to a lepton IC mechanism. In the suggested scenario even if the primary content of the jet is leptonic, the ablated cloud itself may provide protons for the acceleration process. In this paper we do not discuss the specific mechanisms of particle acceleration, but simply assume that both electrons and protons are effectively accelerated during the interaction of the blob with the jet.

3. RADIATION MECHANISMS

In this section we discuss the applicability of different radiation mechanisms responsible for the gamma-ray emission of blazars in the context of the shortest variability timescale of order of 100 s observed during strongest flares of PKS 2155–304. The spectral energy distribution (SED) of the source has a typical shape for such objects with two pronounced humps. The low energy component peaks in the optical-UV-soft X-ray band at $\nu \sim 10^{16}$ Hz, whilst the high energy bump has a maximum in the VHE band. The location of the gamma-ray maximum is measured only in the low state of the source, during simultaneous Fermi-HESS observations in 2009, which revealed a broad maximum between 10 GeV and 100 GeV (Aharonian et al. 2009b). Although the exact position of the gamma-ray maximum is not yet measured in the high state of the source, the observed spectral flattening during the July 2006 flares (Aharonian et al. 2009a) indicates a tendency of the extension of the region of the flux maximum, but most likely not far beyond 100 GeV. Note that for the distance to the source of $D = 540$ Mpc ($z = 0.116$), the attenuation of gamma-rays of energy $\ll 1$ TeV in the extragalactic background light (EBL) is negligible. Therefore throughout this paper we will assume that the gamma-ray peak in the SED of this source is located around 100 GeV. The average apparent gamma-ray luminosity of the 2006 July flares was at the level of $\sim 10^{47}$ erg s $^{-1}$. During the giant July 28 flare, the source was not monitored in the X-ray energy band, but the simultaneous observations of the next night, also characterized by strong flares, conducted with the H.E.S.S., Chandra and Bronberg optical telescope, revealed that the luminosity of the object in optical, UV and X-ray energy bands was an order of magnitude lower compared to the gamma-ray luminosity. These rather general properties of the SED, which include peak location and flux ratio, allow us to derive some important constraints on the production mechanisms.

3.1. Gamma rays associated with electrons

3.1.1. SSC model

In the SSC models the high energy gamma-rays are produced by relativistic electrons through IC scattering of synchrotron radiation of the same electron population. Generally, this model satisfactorily explains the basic features of gamma-ray blazars. However, the ultrafast flares of PKS 2155–304 pose severe constraints on the param-

eters characterizing the gamma-ray production region. Generally, the IC scattering proceeds in the Thomson regime, when $h\nu E_\gamma \ll m^2 c^4 \delta^2$, where $\delta \gg 1$. Thus, in the co-moving reference frame,

$$E_{\gamma,11} = 4 \times 10^{-10} \nu_{16} \gamma^2, \quad (32)$$

where γ is the electron Lorentz factor, $E_{\gamma,11} = E_\gamma/100$ GeV and $\nu_{16} = \nu/10^{16}$ Hz are the peak energies of IC and synchrotron components in the observer reference frame. Then, the electron Lorentz factor can be estimated as

$$\gamma = 5 \times 10^4 \left(\frac{E_{\gamma,11}}{\nu_{16}} \right)^{1/2}. \quad (33)$$

The strength of the magnetic field in the co-moving frame can be defined from the location of the synchrotron peak,

$$\nu = 6 \times 10^6 B_0 \gamma^2 \delta \text{ Hz}, \quad (34)$$

where $B_0 = B/1$ G. Here, for order-of-magnitude estimates, we adopt that the maximum of the νF_ν distribution of synchrotron photons occurs at energy $1.33\omega_c$ ¹, where

$$\omega_c = \frac{3 e B E^2}{2 m^3 c^5}$$

is the synchrotron characteristic frequency, while the maximum of the F_ν distribution is located at a lower energy of $0.29\omega_c$. Thus, one obtains:

$$B_0 = 0.7 \nu_{16}^2 E_{\gamma,11}^{-1} \delta^{-1}. \quad (35)$$

The ratio of the IC and synchrotron peak luminosities, f , is another important parameter characterizing two-hump SEDs:

$$f = \frac{L_{\text{IC}}}{L_{\text{syn}}} = \frac{w_{\text{ph}}}{w_B}. \quad (36)$$

In the SSC model, taking into account the constraint on the size of the production region imposed by the observed variability of the time-scale in Equations (1–3), a lower limit for the co-moving energy density of the target photons can be obtained:

$$w_{\text{ph}} \geq 10^{10} \frac{L_{X,46}}{\tau_2^2 \delta^6} \text{ erg cm}^{-3}, \quad (37)$$

where $L_{X,46} = L_X/10^{46}$ erg s $^{-1}$ is the apparent synchrotron luminosity. For the given luminosity ratio of the observed high and low energy components, one finds

$$\delta \approx 900 \left(\frac{L_{X,46} E_{\gamma,11}^2}{f \tau_2^2 \nu_{16}^4} \right)^{1/4}. \quad (38)$$

Thus, for SEDs, typical for ultrafast flares of PKS 2155–304, the Doppler factor of the relativistically moving gamma-ray source should exceed $\delta \sim 500$. Note that this condition is stronger than the constraint on the Doppler boosting imposed by the condition of the gamma-ray transparency of the source (Begelman et al. 2008).

¹ This energy is in fact used in Equation (32) for IC scattering in the Thomson regime

The order-of-magnitude estimates of Equations (35) and (38), obtained for SSC scenario, suggest that short flares from PKS 2155–304 should be produced at large distances from the BH (given the weak magnetic field and large Doppler boosting factors). This requirement is, in fact, very constraining for JRGI scenario, since the jet ram pressure in this region appears to be extremely small, viz.

$$P_{\text{ram,SSC}} \approx \frac{B_0^2 \Gamma_j^2}{8\pi} \approx 5 \times 10^{-3} \nu_{16}^4 E_{\gamma,11}^{-2} \text{ dyn, cm}^{-2}, \quad (39)$$

which is not enough (by far) to ablate the required amount of stellar material.

The above estimates show that SSC models meet severe limitations in the framework of JRGI scenario due to the required weak magnetic field. We note that the above severe constraints are basically due to the very small magnetic field. In principle, one can assume that the magnetic field in the blob is much weaker than in the jet, which could improve the effect of the SSC mechanism. However, in any case, Equation (38) can be satisfied only at very large distances, where the jet ram pressure is very small and to oblate and accelerate the stellar atmosphere is difficult.

3.1.2. Model of external photon field

The main difference between EIC and SSC models is that in the former one the gamma radiation is dominated by the scattering of electrons on low-energy photons of external origin. Obviously, in such a case the energy density of the external photon field should exceed significantly the energy density of the synchrotron photons, i.e. the photon energy density in the jet vicinity should fulfill the following requirement

$$w_{\text{ext}} \geq 10^{10} \frac{L_{X,46}}{\tau_2^2 \delta^6 \Gamma_j^2} \text{ erg cm}^{-3}, \quad (40)$$

which follows immediately from Equation (37). In fact, even a very weak external photon field can fulfill this requirement, given a very strong dependence on the jet Lorentz factor. Another limitation on the external photon field can be derived from the ratio of the IC and synchrotron peaks (see Equation (36)) which together with Equations (18) and (19) give the following luminosity limit:

$$L_{\text{ext}} \geq 3 \times 10^{42} f L_{j,46} z_{17}^{-1} M_{\text{BH},8} \text{ erg s}^{-1}, \quad (41)$$

which is likely available in the vicinity of powerful blazars. Since this photon field may remain undetectable, the energy of the target photon is, to a large extent, a free parameter. Thus, Equation (32) is not valid in the EIC case, and the model parameters are less constrained than in the SSC scenario. In particular, this allows us to relax the requirement of weak magnetic field, which is crucial for SSC models in the framework of JRGI scenario. To make quantitative estimates, one needs to assume some basic properties of the external field, namely the typical photon energy $\epsilon_{\text{eV}} = \epsilon/1$ eV and its luminosity L_{ext} . Then Equations (32) and (35) obtain the following form:

$$E_{\gamma,11} = 10^{-11} \epsilon_{\text{eV}} \gamma^2 \delta^2, \quad (42)$$

and

$$B_0 = 2 \times 10^{-2} \nu_{16} \epsilon_{\text{eV}} \delta E_{\gamma,11}^{-1}. \quad (43)$$

Together with Equations (18) and (19), one can solve these equations and represent γ and ϵ_{eV} as

$$\epsilon_{\text{eV}} \approx 10 L_{j,46}^{1/2} E_{\gamma,11} M_{\text{BH},8}^{1/2} \nu_{16}^{-1} z_{17}^{-3/2}, \quad (44)$$

and

$$\gamma \approx 1.5 \times 10^3 \nu_{16}^{1/2} z_{17}^{1/4} M_{\text{BH},8}^{1/4} L_{\gamma,46}^{-1/4}. \quad (45)$$

An important characteristic of the model is the emitting particle cooling time in the jet reference frame:

$$t'_{\text{cool}} = 3 \times 10^7 w_0^{-1} \gamma^{-1} \text{ s}, \quad (46)$$

where $w_0 = w_{\text{B}} + w_{\text{ph}} = (f+1)w_{\text{B}}$ is the comoving frame energy density of the target fields in units of erg cm^{-3} . Equations (19) and (45) result in the following cooling time:

$$t'_{\text{cool}} = 3 \times 10^3 (1+f)^{-1} z_{17}^{7/4} L_{j,46}^{-3/4} M_{\text{BH},8}^{-1/4} \nu_{16}^{-1/2} \text{ s}. \quad (47)$$

This fast cooling allows us to relate the observed variability on timescale of several hundred seconds, with the relativistic particle radiation cooling. We note as well that given the relatively low energies of the electrons, $E_e \sim 1 - 10$ GeV, and the strong magnetic field ($B \sim$ few G), the acceleration of these electrons can be easily realized.

Finally, we have to note that the obtained values should fulfill the condition of IC scattering in the Thomson regime: $\gamma \epsilon_{\text{ext}} \Gamma_j \ll mc^2$ (since some used relations, e.g. Equation (42), are valid in the Thomson regime only). This yields the following requirement for the interaction point:

$$z_{17} \gg L_{j,46}^{1/3} M_{\text{BH},8}^{1/3} E_{\gamma,11}^{4/3} \nu_{16}^{-2/3}. \quad (48)$$

In the case that this condition is not true, the interaction of electron with target photons occurs in the Klein-Nishina regime and a few additional effects, such as Klein-Nishina electron losses and gamma-gamma attenuation, have to be taken into account. Actually, since in this case, the Klein-Nishina losses have to be the dominant cooling mechanism, the gamma-gamma absorption is unavoidably large. Indeed, the Klein-Nishina cooling time is

$$t'_{\text{KN}} = \frac{E}{\dot{E}_{\text{KN}}} \approx \frac{1}{cn'_{\text{ext}} \sigma_{\text{KN}}} \approx 10^2 \tau_2 \Gamma_j \text{ s}, \quad (49)$$

where n'_{ext} and σ_{KN} are the target photon density in the jet frame and Klein-Nishina cross-section, respectively. On the other hand, the gamma-gamma optical depth can be estimated as (see Derishev 2009)

$$\tau_{\gamma\gamma} = z n_{\text{ext}} \sigma_{\gamma\gamma} \approx 40 M_{\text{BH},8} \tau_2^{-1}, \quad (50)$$

where n_{ext} and $\sigma_{\gamma\gamma}$ are the target photon density in the laboratory frame and pair-production cross-section. To derive Equation (50), we have used the approximate relation $\sigma_{\gamma\gamma} \approx 2\sigma_{\text{KN}}$ and Equations (18) and (47). Thus, it is rather unlikely that short flares can be produced in the Klein-Nishina regime on the external photon field.

3.2. Gamma rays associated with protons

3.2.1. pp and $p\gamma$ interaction

The production of gamma-rays from interactions of relativistic protons with the surrounding gas is one of the major processes in high energy astrophysics. This process is effective in relatively dense environments, namely when the pp cooling time, $t_{pp} = 10^{15}/n$ s does not exceed other characteristic times (here n is the target proton density in units of cm^{-3}). In the case of the blob in the jet, the most relevant times are the interaction time of the blob with the jet given by Equation (29) (which can be treated as the acceleration time of protons), and the escape time of protons from the blob. The number density of protons in the blob is constrained by Equations (21) and (25). For the parameter values expected in the scenario, the number density of protons does not exceed 10^4 cm^{-3} . The corresponding pp cooling time of $\geq 10^{11}$ s is too long, and does not leave any room for the explanation of the variability of TeV radiation on any observed time-scale. Even the assumption that the variability is caused by other reasons, e.g. due to the adiabatic cooling or change of the Doppler factor, cannot help much since in this case, an extremely low efficiency represents an unavoidable argument against this process.

The efficiency of gamma-ray production can be much higher through other channels related to interactions with the radiation and magnetic fields. In both cases the gamma-ray production rate increases dramatically with the energy of protons, and achieves reasonably high efficiency if the protons are accelerated to energies of 10^{19} eV or beyond. For the compact blobs with linear dimensions severely constrained by the hour-long or shorter variability timescales, the energy of protons can achieve such high energies only when the particle acceleration proceeds (1) at a rate close to the theoretical limit, $t_{\text{acc}} \sim r_L/c$ and (2) in the presence of a magnetic field as large as 100 G (Aharonian 2000). Whilst for these conditions both the acceleration and synchrotron cooling times in the frame of the blob can be as short as 1h, the fast cooling of protons via photomeson interactions require very dense photon fields at mm and far-infrared wavelengths. On the other hand, the density of the radiation field (of internal or external origin) is constrained by the condition of transparency of the production region for the VHE gamma-rays, implying that the optical depth regarding the photon-photon pair production cannot significantly exceed unity. This condition, coupled with the condition of a large magnetic field amplitude of $B \sim 100$ G, makes the cooling time of protons via photomeson processes significantly longer compared to the proton synchrotron cooling time (Aharonian 2000). Although, formally one can “construct” a model with extreme parameters, where the photomeson processes could compete with the proton synchrotron cooling, below we will focus our treatment on the production of gamma-rays via synchrotron radiation.

3.2.2. Proton synchrotron radiation

Protons of extremely high energy and large magnetic fields strengths are the two conditions which make proton synchrotron an effective radiation mechanism. If these conditions are satisfied, the spectrum of synchrotron radiation can extend to the gamma-ray domain with a char-

acteristic energy (Aharonian 2000):

$$E_{\gamma,11} \approx 1 B_2 E_{19}^2, \quad (51)$$

where $E_{19} = E/10^{19}$ eV is the proton energy, and $B_2 = B/100$ G is the strength of the magnetic field. The position of the peak depends strongly on the maximum energy of protons, which is determined by the balance between the particle acceleration and cooling rates. It is convenient to present the acceleration time of the protons, independent of the specific mechanism of acceleration, in the form:

$$t_{\text{acc}} = \frac{\eta(E)r_L}{c} \approx 10^4 E_{19} B_2^{-1} \eta(E) \text{ s}, \quad (52)$$

where $r_L = E/eB = 3 \times 10^{14} B_2 E_{19} \text{ cm}$ is the so-called gyro-factor. We note that this value is remarkably close to the required size of the blob in the JRG scenario (see Equation (25)). The dimensionless parameter, $\eta(E) \geq 1$, in Equation (52) characterizes the acceleration efficiency; the most efficient acceleration occurs for $\eta = 1$. It is believed that the acceleration by relativistic shocks (see e.g. Achterberg et al. 2001) or at the annihilation of the magnetic field lines (Haswell et al. 1992) occurs in the regime when $\eta \sim 1$. In a more general context, the relativistic outflows found in AGN and GRBs, which presently are considered as most feasible sites of the production of the highest energy cosmic rays, can accelerate protons to 10^{20} eV only if $\eta \sim 1$ (Aharonian et al. 2002). In the comoving frame, the characteristic synchrotron cooling time of the protons is:

$$t_{\text{sy}} = \frac{4\pi m_p^4 c^3}{\sigma_T m_e^2 E B^2} = 3 \times 10^4 B_2^{-2} E_{19}^{-1} \text{ s}. \quad (53)$$

From comparison of the acceleration and cooling rates one finds a maximum energy of protons of;

$$E_{p,\text{max}} = 1.7 \times 10^{19} B_2^{-1/2} \eta^{-1/2} \text{ eV}, \quad (54)$$

and a corresponding maximum energy of synchrotron photons of;

$$E_{\gamma,\text{max}} = 400 \eta^{-1} \text{ GeV}. \quad (55)$$

If synchrotron radiation is emitted by a blob with a Doppler-factor, δ , the peak of the synchrotron radiation is shifted to

$$E_{\gamma,\text{max}} \approx 400 \eta^{-1} \delta \text{ GeV}. \quad (56)$$

One can see that for a Doppler factor of $\delta \leq 100$, synchrotron radiation can extend to TeV energies provided that the proton acceleration rate is close to $\eta \leq 100$.

Another important constraint can be obtained through so-called *Hillas criterion*, i.e. a requirement for the size of the acceleration site to be larger than the gyroradius of the highest energy particles. Substituting Equations (19) and (54) into the Larmor radius, $r_L \approx E/eB_c$, one obtains

$$\zeta_{17}^{3/2} L_{\gamma,47}^{-1/2} L_{j,46}^{-1/4} \eta_1^{-1/2} \xi_{-1}^{1/2} M_{\text{BH},8}^{-1} < 0.1. \quad (57)$$

Here the size of the acceleration site was assumed to be defined by Equation (25). A significantly more severe constraint for the proton synchrotron models comes from

the cooling time requirement. Namely, the expected variability time scale can be estimated from Equations (18), (19), (53) and (54):

$$\tau_{\text{psyn}} \approx \frac{t_{\text{sy}}}{\delta} \approx 2 \times 10^4 \eta_1^{1/2} M_{\text{BH},8}^{1/2} z_{17}^{-3/4} L_{j,46}^{-3/4} \text{ s}. \quad (58)$$

Thus, in the case of powerful jets, $L_j > 10^{47} \text{ erg s}^{-1}$, the proton synchrotron mechanism can guarantee variability on time-scales of several hundred seconds.

Although a detailed study of broad-band SED in the framework of proton synchrotron scenario remains outside of the scope of this paper, below we outline some expected features. In particular, one may expect that the acceleration of protons is accompanied by the acceleration of electrons, whose particle population may create a detectable nonthermal emission component. Due to more effective synchrotron losses, the maximum energy of electrons is rather small:

$$E_e = 5B_2^{-1/2} \eta_e^{-1/2} \text{ TeV}. \quad (59)$$

The corresponding synchrotron peak appears at an energy, which is by a factor of m_p/m_e smaller than the peak energy of proton synchrotron (see Equation (56)):

$$E_{\text{syn}} \approx 150\eta_e^{-1} \text{ MeV}. \quad (60)$$

Thus, in this scenario, the synchrotron peak of electrons, additionally boosted by the value of the Doppler factor, $\delta \sim 50$, is expected at GeV energies, but not in the traditional X-ray radiation band. In this regard the so-called synchrotron peak, which in TeV blazars is located in the UV to X-ray band, needs a new (non-standard) interpretation in the framework of our model. Finally, it is important to note that the flux ratio of proton to electron synchrotron peaks depends on the ratio of the injection rates of those particles, which is an highly uncertain parameter.

The peak of soft radiation in the region of 10^{16} Hz can be produced by secondary electrons produced in interactions of VHE gamma-rays with soft photons. A modest absorption of VHE gamma-rays cannot be excluded. Moreover, in the case of blazars with extremely hard TeV source spectra (i.e. after correction for the intergalactic absorption), the energy-dependent absorption can be a natural explanation of the unusually hard gamma-ray spectra (Aharonian et al. 2008; Zacharopoulou et al. 2011).

The energy of the absorbed gamma-ray photon is shared between an e^\pm pair, so each electron on average gets the half of the original energy, i.e., $E_e \sim E_\gamma/2$. Generally, synchrotron radiation of secondary electrons produced inside the jet will be Doppler boosted, therefore this amplified component of synchrotron radiation can be detected by the observer. The peak energy of the secondary synchrotron radiation is quite sensitive to the Doppler factor of the blob and the energy spectrum of the parent gamma-rays. For the standard values used in this paper, the peak of the synchrotron radiation can vary in a quite broad interval between UV and hard X-ray (Zacharopoulou et al. 2011).

Thus within the suggested scenario, we expect a broad-band SED consisting of three synchrotron peaks of different origin located at the keV, MeV/GeV and TeV bands. Schematically, such a SED is shown in Figure 4. While

the amplitudes of the MeV and TeV synchrotron peaks are determined by the total energy accelerated in the form of electrons and protons, respectively, the intensity of the low energy synchrotron peak is determined by the fraction of absorbed TeV (proton-synchrotron) gamma-rays.

4. APPLICATION TO PKS 2155–304

In the case of the July 2006 flares of PKS 2155–304 the total energy of the nonthermal radiation detected during the burst was about $E_{\text{tot}} \approx L_\gamma \Delta t \approx 10^{51} \text{ erg}$. According to Equation (30), such an energy release can be produced by an ensemble of clouds satisfying to the following condition:

$$\xi_{-1} M_{c,25} \Gamma_{j,1.5}^3 \approx 10. \quad (61)$$

This requirement can be easily fulfilled given the large mass of material, that can be accelerated by the jet. Indeed, for the mass obtained through Equation (21), the above condition is reduced to:

$$L_{j,46} > 0.5 \frac{1}{\xi_{-1} M_{\text{BH},8} \Gamma_{j,1.5}^2}. \quad (62)$$

The detected short variability of $\tau \sim 200 \text{ s}$ implies some additional constraints on the system parameters. The causality condition constrains the size of the blob $r_c \approx \delta \tau c \approx \Gamma_j \tau c$ (here we assume the size of the production region to be $2r_c$ and $\delta = 2\Gamma_j$). This allows one to relate the variability time-scale and the peak luminosity through Equation (23):

$$L_{j,46} > 30 \frac{M_{\text{BH},8}^2 L_{\gamma,47}}{\tau_2^2 \Gamma_{j,1.5}^2 \xi_{-1}}. \quad (63)$$

In the specific case of PKS 2155–304, this condition implies a lower limit on the jet power, $L_j > 10^{47} M_{\text{BH},8}^2 \Gamma_{j,1.5}^{-2} \xi_{-1}^{-1} \text{ erg s}^{-1}$. Since the Eddington luminosity has the following value $L_{\text{Ed}} \approx 1.4 \times 10^{46} M_{\text{BH},8} \text{ erg s}^{-1}$, the jet should have a super Eddington luminosity, unless the bulk Lorentz factor is large, i.e. $\Gamma_j > 75 M_{\text{BH},8}^{1/2} \xi_{-1}^{-1/2}$.

In the framework of JRGI scenario, the above conditions are quite general and do not depend on the radiation mechanism. Obviously, the available energy has to be transferred to gamma-rays by a radiation mechanism with an adequate cooling time. It was shown in Section 3 that, in general, both leptonic (EIC) and hadronic (proton synchrotron) mechanisms can be quite efficient in the frameworks of the JRGI scenario. Below we check the feasibility of these two mechanisms for the specific case of PKS 2155–304; namely, we combine the energy and variability constraints with radiation mechanism specific limitations (e.g. cooling time).

4.1. EIC model for PKS 2155–304

Given the short cooling time in the case of EIC (see Equation (47)), the required variability can be achieved for a relatively low jet luminosity:

$$L_{j,46} > 0.007 \frac{M_{\text{BH},8}^2 \Gamma_{j,1.5}^{10/3}}{\tau_2^{4/3} \nu_{16}^{2/3}}. \quad (64)$$

On the other hand, the IC scattering should occur in the Thomson regime, otherwise the gamma-gamma opacity would significantly exceed unity (see Equation (50)). Thus, Equation (48) allows the following upper limit on the jet luminosity:

$$L_{j,46} \ll 0.4 \frac{M_{\text{BH},8}^2 \Gamma_{j,1.5}^6 \nu_{16}^2}{E_{11}^4}, \quad (65)$$

which appears to be rather close to the lower limit given by Equation (63). For the sake of clarity, we have combined all the relevant limitations in Figure 5, where the favorable parameters are indicated by the filled region. It is expected that the EIC mechanism can be responsible for nonthermal emission with the required characteristics in the case of sub-Eddington jets. On the other hand, the EIC model requires less comfortable bulk Lorentz factor, which for the radiation production region should exceed $\Gamma_j > 75$. In the framework of the JRGI scenario this implies that the star enters into the jet quite far from the BH, $z > 4 \times 10^{17} M_{\text{BH},8}$ cm. Finally, we note that the EIC model does not pose a strict requirement on the acceleration process given the relatively small energy of the emitting electron.

4.2. Proton synchrotron model for PKS 2155–304

One of the most fundamental challenges for proton synchrotron models in AGN jets is the long cooling time. This is often interpreted as an indication of the extremely low efficiency of such models. In particular, Sikora (2010) has compared the synchrotron cooling time to the expected adiabatic cooling time in relativistic jets. Based on this comparison, it was concluded that this mechanism was not feasible for nonthermal photon production in AGN jets. However, we note that this estimate depends strongly on the key assumption of the jet magnetization. This parameter has been accepted to be quite low by Sikora (2010), whilst in this paper, we rely on models of magnetically driven jets, i.e. the magnetization can be very high. Given the large magnetic field, proton synchrotron radiation from jets can be quite efficient in our scenario.

The cooling time for proton synchrotron radiation, Equation (58), recall for a very luminous jet

$$L_{j,46} > 500 \frac{M_{\text{BH},8}^2 \Gamma_{j,1.5}^{8/3} \eta_1^{2/3}}{\tau_2^{4/3}}. \quad (66)$$

Note that, Equations (62), (63) and (66) together require quite an extreme jet luminosity, but the requirement may be relaxed in the case of relatively small bulk Lorentz factors, i.e., $\Gamma_j \approx 20$. Although even in this case, the jet luminosity exceeds the Eddington luminosity. The relevant parameter space is shown by the filled region in Figure 7. This corresponds to the case when the JRGI scenario is realized relatively close to the base of the jet, $z \approx 3 \times 10^{16} M_{\text{BH},8}$ cm. Finally, we note that proton synchrotron models require a very efficient particle acceleration with a rate close to the theoretical electrodynamic limit, i.e. $\eta \leq 10$. The corresponding Doppler factor can be as high as $\delta \gtrsim 40$. One should expect a cutoff in the gamma-ray spectrum at around $\approx 1.5 \eta_1^{-1}$ TeV. Thus, the observed VHE spectrum, extending up to 4 TeV, requires an acceleration parameter of $\eta \leq 10$.

This implies that the proton synchrotron model can be realized only in extreme accelerators.

5. DISCUSSION

The ultra-short TeV gamma-ray flares of blazars detected in the case of PKS 2155–304 (Aharonian et al. 2007) and Mkr 501 (Albert et al. 2007) on 100 s timescales represent a serious challenge for current models of blazars. This challenge concerns the origin and the sites of formation of these flares, the acceleration and radiation mechanisms, the hydrodynamics of relativistic outflows, amongst others. Since the upper limit on the size of production region, of $3 \times 10^{12} \tau_2$ cm, is smaller by an order of magnitude than the gravitational radius of a black hole of mass $10^8 M_\odot$ (which is required to power distant blazars), the only way to avoid the situation of invoking quite uncomfortable upper limits on the mass of the central black hole (as small as $10^7 M_\odot$), is to invoke the Doppler boosting. However, this can be realized only in the case of an external origin of the processes which cause these ultra-short flares. If the flares are initiated by disturbances originating from the central black hole (e.g., due to internal shocks), the linear size (in the observer’s frame) of the flare production region cannot be smaller than the gravitational radius of the black hole, independent of the Doppler factor of the jet. The model suggested in this work readily solves the problem of connecting the flares to the interactions of the red giant stars with the powerful jets. Due to these interactions the red giant loses a significant fraction its atmosphere. The cloud, accelerated by the magnetically driven jet up to a Lorentz factor of $\Gamma \sim 30$, likely separates into many small fragments. These “blobs” represent the ideal sites for the production of flares, provided that a significant fraction of jet energy absorbed by the cloud is converted (e.g. due to relativistic shock acceleration or magnetic reconnection) to relativistic particles.

The effective acceleration of particles is a necessary, but not a sufficient condition for the interpretation of the gamma-ray radiation of blazars. Any successful model of TeV blazars require adequate cooling times through gamma-radiation; they should be comparable, or often even shorter compared to the characteristic timescales of other radiative and non-radiative processes. Generally, leptonic models of gamma-ray loud blazars, through the realization of SSC or external IC scenarios, do provide adequate radiation timescales, but at the expense of the assumption of a rather weak magnetic field, typically less than 1 G, which in powerful blazars ($L_j \geq 10^{46}$ erg s $^{-1}$), is well below the magnetic field in the jet as long as it’s concerned with sub-parsec distances (see Figure 3). This is a quite challenging requirement of the discussion of feasibility of, which is generally ignored in the literature. In the JRGI scenario suggested here the problem can be formally solved assuming that the magnetic field inside the blob is much smaller than in the jet. However, in the case of the SSC models, this assumption still does not allow a relaxation of the second requirement of an extremely large jet Lorentz factor, $\Gamma \geq 1000$. Although such Lorentz factors for the bulk motion cannot be excluded², in particular at large, ≥ 1 pc distances from the BH (see Figure 3), in the proposed JRGI model it hardly

² We should note that it is rather difficult to reach such a high

can work. At such distance the jet ram pressure is not sufficient able to ablate the atmosphere of the star.

The requirements on the magnetic field and the jet Lorentz factor are more relaxed in the external IC model. Nevertheless, one should note that within the JRGI scenario, the external Compton model has some specific features. In order to avoid severe gamma-gamma absorption, the Compton scattering should proceed in the Thomson regime. This can be fulfilled if the radiation region is located at large distances, i.e. regions still with quite a large Lorentz factors for the jet, $\Gamma_j \sim 100$.

One of the main postulates of the JRGI scenario is the effective star-jet interaction. This requires the location of the blobs that emit gamma-rays to be at small distances from the BH, typically $z \sim 10^{17}$ cm. In the case of powerful jets, $L_j \geq 10^{47}$ erg s $^{-1}$, this implies a very large magnetic field, $B \sim 100$ G and a moderate Lorentz factor, $\Gamma_j \sim 20$. Both parameters match nicely with the interpretation of the TeV gamma-ray flares as a result of proton-synchrotron radiation by highly magnetized blobs, formed and accelerated in jet-star interactions. This model demands the acceleration of protons to energies of 10^{19} eV, and implies the acceleration of protons with a rate close to the maximum (theoretically possible) rate of, $t_{\text{acc}} \sim r_L/c$. This is quite a robust requirement, which however, can be provided, in principle, by certain acceleration mechanisms. Another challenge of the proposed scenario is related to the power of the jet. Namely, the proton synchrotron model of TeV gamma-rays can be effective, provided that: (i) the mass of BH does not significantly exceed $M \sim 10^8 M_\odot$ and; (ii) the jet power is not significantly below 10^{47} erg s $^{-1}$. An unambiguous implication of these two requirements (working in two different directions) is that the jet should have a super-Eddington luminosity. Although this could seem like quite a dramatic assumption, we note the requirement of super-Eddington luminosities seems to be

an unavoidable, model-independent conclusion for GRBs and also likely for powerful gamma-ray blazars (Ghisellini 2011).

5.1. Stellar density in the vicinity of a SMBH.

An important question in the suggested scenario is the expected rate of the flaring events, which is related to the number density of RGs at the relevant jet scales. The jet region suitable for the production of the powerful flares (similar to the burst detected from PKS 2155–304), can be defined as $z < 1$ pc, and the corresponding side cross section of the jet is $S_j \approx z^2 \theta \sim 10^{33} \theta_{-1} z_{17}^2 \text{cm}^2$. Thus, the number of flaring events per year can be estimated as $\Upsilon \approx S_j V_{\text{orb}} n$. Equation (8) provides an estimate for the density of RGs required to produce Υ flaring events per year:

$$n \sim 10^6 \Upsilon M_{\text{BH},8}^{-1/2} \theta_{-1}^{-1} z_{17}^{-3/2} \text{pc}^{-3}. \quad (67)$$

Unfortunately, there are no direct measurements of the stellar density in the vicinity of BHs. Thus, depending on the assumed distribution law, the number of RGs in the vicinity of the BH may or may not be sufficient. However, we note that studies of possible stellar density profiles in the vicinity of the BH in AGNs (see e.g. (Bisnovatyi-Kogan et al. 1982; Murphy et al. 1991)) show that densities similar to the one required ($\sim 10^6 \text{pc}^{-3}$) are rather feasible. Moreover, under the influence of X-ray radiation close to BHs, normal stars can drastically increase the rate of their stellar wind. Thus, wind-fed clouds can be formed during the jet – star interaction. This interaction can mimic the interaction of RG atmosphere with the jet (Dorodnitsyn, private communications). Since, the stellar density of normal stars is higher up to 2 orders of magnitude than the density of RGs, this effect can significantly relax the requirement imposed by Equation (67) on the stellar density in the vicinity of BHs.

APPENDIX

DERIVATION OF THE CLOUD DYNAMICS EQUATION IN THE RELATIVISTIC STAGE

Let us choose the orientation of coordinate systems such that in the observer reference frame, K , the magnetic and electric field vectors have the following components $\mathbf{B} = (0, B, 0)$ and $\mathbf{E} = (E, 0, 0)$, respectively. Since the conductivity of plasma is very high, the following condition is held $E = v_j B/c$, where v_j is jet velocity. The cloud velocity in the system K is v_c , and K' is the cloud's momentarily comoving reference frame. Quantities pertaining to the system K' are marked by prime. In the system, K' electromagnetic field strengths are

$$E' = \Gamma_c \left(E - \frac{v_c}{c} B \right) = \frac{1}{c} \Gamma_c (v_j - v_c) B, \quad (A1)$$

$$B' = \Gamma_c \left(B - \frac{v_c}{c} E \right) = \Gamma_c \left(1 - \frac{v_j v_c}{c^2} \right) B. \quad (A2)$$

As it should be, the following ratio holds; $E'/B' = v'_j/c$, where v'_j is the jet speed relative to the cloud. Energy flux density in system K' and in the laboratory system are related by:

$$q' = \frac{c}{4\pi} E' B' = \frac{1}{c} \Gamma_c^2 (v_j - v_c) (1 - v_j v_c / c^2) q. \quad (A3)$$

Jet ram pressure in the system K' is equal to q'/c , thus during a differentially small time interval, dt' , the cloud momentum increases by a value of $dP'_c = (q'/c) \pi r_c^2 dt'$, and the energy increment is a second order value of dt' , i.e. $dE'_c = 0$. In the observer system, one has $dE_c = M_c c^2 d\Gamma_c = \Gamma_c v_c dP'_c$, and $dt = \Gamma_c dt'$. Thus, the equation of motion

value of the bulk Lorentz factor, e.g. due to the so called “photon

breeding mechanism” (Stern & Poutanen 2006), which does not allow AGN jets with bulk Lorentz factors exceeding 50.

may be expressed as follows:

$$\frac{d\Gamma_c}{dt} = \frac{\pi r_c^2 v_c}{M_c c^3} q' = \frac{\pi r_c^2}{M_c c^4} v_c \Gamma_c^2 (v_j - v_c) (1 - v_j v_c / c^2) q. \quad (\text{A4})$$

Denoting $q = L_j / \pi \omega^2$ and assuming $\Gamma_j \gg 1$ and $\Gamma_c \gg 1$, one obtains the equation of motion in the form of Equation (12)

$$\frac{d\Gamma_c}{dt} = \left(\frac{1}{\Gamma_c^2} - \frac{\Gamma_c^2}{\Gamma_j^4} \right) \frac{L_j r_c^2}{4 \omega^2 c^2 M_c}, \quad (\text{A5})$$

THE VARIATION OF δ IN THE CASE OF BLOB CHAOTIC MOTION

In the suggested scenario, non-thermal particle acceleration is triggered by RG material blobs caught up in the jet. In such a case it is natural to assume that the acceleration sites are closely related to the blobs. Although the particle propagation and isotropisation processes may be very complicated, the highest energy particles lose their energy very close to the acceleration site. Thus, in what follows we assume that the VHE emission is related to the blobs and the radiation boosting factor is determined by the blob velocity. Since the blob velocity can be changed relatively easy, sudden changes of the Doppler factor are rather feasible. Hence we have discuss the related changes of the Doppler factor and *correction function* F_e , i.e. the quantities describing the non-thermal emission intensity, as seen by observer.

A

Let us assume that at the moment t_0 , a blob moves relativistically in the direction of the observer with velocity $V = \beta c$, thus, the corresponding Lorentz factor is $\Gamma = 1/\sqrt{1 - \beta^2} \gg 1$. Let us consider two reference frames: the observer coordinate system K , and the blob comoving system K' , where the blob is at rest at t_0 . The z axes are selected to be parallel to the systems' relative velocity, \mathbf{V} . Let us consider two cases for a change of the blob velocity.

In the K' reference frame, the blob gains velocity \mathbf{v}' , such as:

$$v'_x = c\beta' \sin \phi, \quad v'_y = 0, \quad v'_z = c\beta' \cos \phi. \quad (\text{B1})$$

Here ϕ is the angle between the velocity \mathbf{v}' and z' axis; $\beta' \equiv v'/c$; and the observer detects the emission radiated along z axis. In the laboratory frame, the blob velocity components have the following form:

$$v_x = \frac{c}{\Gamma} \frac{\beta' \sin \phi}{1 + \beta\beta' \cos \phi}, \quad v_y = 0, \quad v_z = c \frac{\beta + \beta' \cos \phi}{1 + \beta\beta' \cos \phi}. \quad (\text{B2})$$

Therefore, the blob Lorentz factor is $\tilde{\Gamma} = 1/\sqrt{1 - (v_x^2 + v_y^2 + v_z^2)/c^2}$. Given that the system is in the ultrarelativistic regime (in the Appendixes we will assume $\Gamma \gg 1$), one obtains that the Doppler factor is:

$$\delta = \left[\tilde{\Gamma} (1 - v_z/c) \right]^{-1} = \frac{2\Gamma \sqrt{1 - \beta'^2}}{1 - \beta' \cos \phi}. \quad (\text{B3})$$

In the laboratory frame the velocity deflection angle is $\delta\theta = \beta' \sin \phi / \Gamma \ll 1$. Thus, the Lorentz factor of the radial (i.e. along the z axis) motion Γ_z can be expressed as

$$\Gamma_z \equiv \frac{1}{\sqrt{1 - v_z^2/c^2}} = \Gamma \sqrt{\frac{1 + \beta' \cos \phi}{1 - \beta' \cos \phi}}. \quad (\text{B4})$$

The radiation intensity is defined by the *correction function*, if the time-scale of the blob velocity variation is longer than the typical particle acceleration time. In the case of $\Gamma_j \gg \Gamma_c \gg 1$, one obtains

$$r(\phi) = \frac{\delta^4}{\Gamma_z^2} = \frac{16\Gamma^2 (1 - \beta'^2)^2}{(1 + \beta' \cos \phi)(1 - \beta' \cos \phi)^3}, \quad (\text{B5})$$

Otherwise (i.e. if the particle cooling time is long as compared to the time-scale of the velocity change), the apparent luminosity is proportional to the standard factor δ^4 . Thus, one obtains

$$r(\phi) = \delta^4 = \frac{16\Gamma^4 (1 - \beta'^2)^2}{(1 - \beta' \cos \phi)^4}. \quad (\text{B6})$$

As it can be seen from the comparison of Equations (B5) and (B6), the function r has a weak dependence on the velocity change. At the moment t_0 , this function has a value of $r_0 \equiv r(\phi)|_{\beta'=0} = 16\Gamma^2$. The change of the velocity may lead both to an increase and decrease of the function $r(\phi)$: if $\phi = 0$ and $\beta' \geq 1/3$, the correction function value is $r(0) \geq 2r_0$; and if $\phi = \pi/2$ and $\beta' \geq 0.54$, one has $r(\pi/2) \leq r_0/2$.

B

Another potentially important situation occurs when a blob moves along a helical trajectory, e.g. along the dominant magnetic field line. In this case, the additional velocity component is oriented perpendicularly to the averaged velocity, i.e. its components may be expressed as the follows:

$$v'_x = c\beta' \cos \phi, \quad v'_y = c\beta' \sin \phi, \quad v'_z = 0. \quad (\text{B7})$$

Obviously, if an observer is located in the direction of the z' axis, no flux variability is detected. On the other hand, if the observer is located slightly off axis, a periodic increase of the flux level is seen. Let us assume that the observer is located in the direction of the blob motion for $\phi = 0$. In this case, the Doppler factor has the following form:

$$\delta = \frac{2\Gamma\sqrt{1-\beta'^2}}{1-\beta'^2(2\cos\phi-1)}. \quad (\text{B8})$$

The radiation intensity, then, is proportional to the following factor:

$$r = \frac{\delta^4}{\Gamma^2} = \frac{16\Gamma^2(1-\beta'^2)^2}{(1-\beta'^2(2\cos\phi-1))^4}. \quad (\text{B9})$$

Obviously, the maximum value of r is achieved when $\phi = 0$, i.e. when the radiation is emitted towards the observer. If the precession velocity fulfills the following condition

$$\tilde{\beta}' > \left(\frac{2^{1/4} - 1}{2^{1/4} + 1 - 2\cos\phi} \right)^{1/2}, \quad (\text{B10})$$

then at the corresponding moment, the emission intensity can differ by a factor of 2 as compared to the maximum. For example, if $\phi = \pi/4$ then the required velocity value is $\tilde{\beta}' \approx 0.5$. In Figure 9 we show the ϕ -angle dependence of the normalized intensity for several different values of β' .

Another important issue is the time modulation of the emission, as seen in the observer reference frame. Let us assume that the azimuthal angle has the following time dependence; $\phi = \omega t'$, where ω is a constant; and t' is time in the system K' . Then a quantity $T_0 = 2\pi/\omega$ corresponds to the precession period in the system K' . Obviously, in the observer frame the emission intensity should have a different time dependence than the one that can be obtained by the substitution of $\phi = \omega t'$ into the function shown in Figure 9. Indeed, the radiation emitted at time t_r , by the source is detected by an observer located at $\mathbf{r} = r\mathbf{n}$ at time t , where

$$t = t_r + |\mathbf{r} - \mathbf{r}(t_r)|/c \approx t_r + r/c - (\mathbf{n}\mathbf{r}(t_r))/c, \quad (\text{B11})$$

where $\mathbf{r}(t_r)$ is the emitter position at time t_r . Since the constant term r/c can be neglected, Equation (B11) can be reduced to the following form:

$$t = t_r - (\mathbf{n}\mathbf{r}(t_r))/c. \quad (\text{B12})$$

For K -frame quantities, the azimuthal angle can be represented as $\phi = \omega t_r/\Gamma$. This relationship allows us to express t through ϕ :

$$t = \frac{T_0(1+\beta'^2)}{4\pi\Gamma} \left(\phi - \frac{2\beta'^2}{1+\beta'^2} \sin\phi \right). \quad (\text{B13})$$

By increasing ϕ by 2π , the time, t , changes by an amount equivalent to:

$$T = \frac{T_0(1+\beta'^2)}{2\Gamma}, \quad (\text{B14})$$

which is the period of the observed emission. The dependence of the observed intensity, as a function of the observer time, is shown in Figure 10. As it can be seen from this figure, the distribution width decreases with an increase of β' . The emission ‘‘half-decay’’ interval, $\Delta t/2$, is shown in Figure 11 as a function of β' .

ACKNOWLEDGMENTS

The work of S.V.Bogovalov have been supported by the Federal Targeted Program ‘‘The Scientific and Pedagogical Personnel of the Innovative Russia’’ in 2009-2013 (the state contract N 536 on May 17, 2010)

REFERENCES

- Achterberg, A., Gallant, Y. A., Kirk, J. G., & Guthmann, A. W. 2001, MNRAS, 328, 393
 Aharonian, F., et al. 2007, ApJ, 664, L71
 —. 2009a, A&A, 502, 749
 —. 2009b, ApJ, 696, L150
 Aharonian, F. A. 2000, New Astronomy, 5, 377
 Aharonian, F. A., Belyanin, A. A., Derishev, E. V., Kocharovsky, V. V., & Kocharovsky, V. V. 2002, Phys. Rev. D, 66, 023005
 Aharonian, F. A., Khangulyan, D., & Costamante, L. 2008, MNRAS, 387, 1206
 Albert, J., et al. 2007, The Astrophysical Journal, 669, 862
 Araudo, A. T., Bosch-Ramon, V., & Romero, G. E. 2010, A&A, 522, A97+

- Barkov, M. V., Aharonian, F. A., & Bosch-Ramon, V. 2010, ArXiv e-prints
- Barkov, M. V., & Komissarov, S. S. 2008, *International Journal of Modern Physics D*, 17, 1669
- Begelman, M. C., Fabian, A. C., & Rees, M. J. 2008, *MNRAS*, 384, L19
- Beskin, V. S. 2010, *Physics-Uspehi*, 180, 1241
- Beskin, V. S., & Nokhrina, E. E. 2006, *MNRAS*, 367, 375
- Bisnovatyi-Kogan, G. S., Churaev, R. S., & Kolosov, B. I. 1982, *A&Ap*, 113, 179
- Blandford, R. D., & Znajek, R. L. 1977, *MNRAS*, 179, 433
- Derishev, E. V. 2009, *International Journal of Modern Physics D*, 18, 1523
- Dermer, C. D., Finke, J. D., Krug, H., & Böttcher, M. 2009, *ApJ*, 692, 32
- Ghisellini, G. 2011, ArXiv e-prints
- Giannios, D., Uzdensky, D. A., & Begelman, M. C. 2009, *MNRAS*, 395, L29
- Gregori, G., Miniati, F., Ryu, D., & Jones, T. W. 2000, *ApJ*, 543, 775
- Haswell, C. A., Tajima, T., & Sakai, J. 1992, *ApJ*, 401, 495
- Jorstad, S. G., Marscher, A. P., Mattox, J. R., Wehrle, A. E., Bloom, S. D., & Yurchenko, A. V. 2001, *ApJS*, 134, 181
- Jorstad, S. G., et al. 2005, *AJ*, 130, 1418
- Komissarov, S. S., Barkov, M., & Lyutikov, M. 2007a, *MNRAS*, 374, 415
- Komissarov, S. S., Barkov, M. V., Vlahakis, N., & Königl, A. 2007b, *MNRAS*, 380, 51
- Komissarov, S. S., Vlahakis, N., & Königl, A. 2010, *MNRAS*, 407, 17
- Komissarov, S. S., Vlahakis, N., Königl, A., & Barkov, M. V. 2009, *MNRAS*, 394, 1182
- Levinson, A., & Bromberg, O. 2008, *International Journal of Modern Physics D*, 17, 1603
- Lobanov, A. P. 1998, *A&A*, 330, 79
- Lovelace, R. V. E. 1976, *Nature*, 262, 649
- Marscher, A. P., et al. 2008, *Nature*, 452, 966
- . 2010, *ApJ*, 710, L126
- McKinney, J. C., & Uzdensky, D. A. 2010, ArXiv e-prints
- Murphy, B. W., Cohn, H. N., & Durisen, R. H. 1991, *ApJ*, 370, 60
- Nakamura, F., McKee, C. F., Klein, R. I., & Fisher, R. T. 2006, *ApJS*, 164, 477
- O'Sullivan, S. P., & Gabuzda, D. C. 2009, *MNRAS*, 400, 26
- Pittard, J. M., Hartquist, T. W., & Falle, S. A. E. G. 2010, *MNRAS*, 405, 821
- Ruffini, R., & Wilson, J. R. 1975, *Phys. Rev. D*, 12, 2959
- Savolainen, T., Wiik, K., Valtaoja, E., & Tornikoski, M. 2008, in *Astronomical Society of the Pacific Conference Series*, Vol. 386, *Extragalactic Jets: Theory and Observation from Radio to Gamma Ray*, ed. T. A. Rector & D. S. De Young, 451–+
- Sikora, M. 2010, ArXiv e-prints
- Sokolovsky, K. V., Kovalev, Y. Y., Lobanov, A. P., Savolainen, T., Pushkarev, A. B., & Kadler, M. 2010, ArXiv e-prints
- Stern, B. E., & Poutanen, J. 2006, *MNRAS*, 372, 1217
- Tavecchio, F., Ghisellini, G., Bonnoli, G., & Ghirlanda, G. 2010, *MNRAS*, 405, L94
- Tavecchio, F., Ghisellini, G., Ghirlanda, G., Costamante, L., & Franceschini, A. 2009, *MNRAS*, 399, L59
- Tchekhovskoy, A., Narayan, R., & McKinney, J. C. 2010, *New Astr.*, 15, 749
- Zacharopoulou, O., Khangulyan, D., Aharonian, F. A., & Costamante, L. 2011, *ApJ*, 738, 157

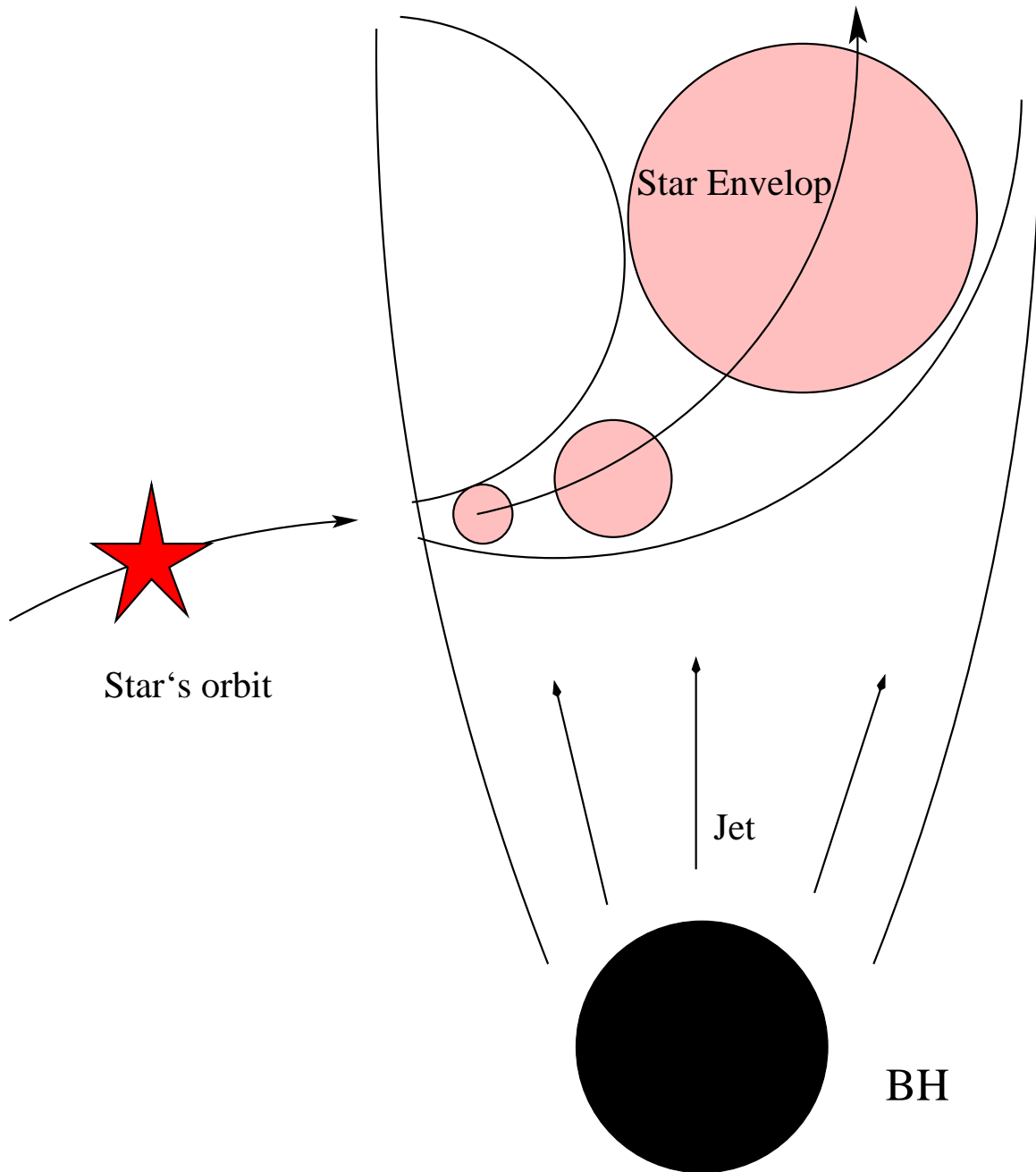


FIG. 1.— Schematic illustration of the scenario. If a star enters a powerful AGN jet, the outer layers of the star atmosphere are to be ablated. Because of the interaction with the jet the ablated cloud expands and gets involved into the jet bulk motion.

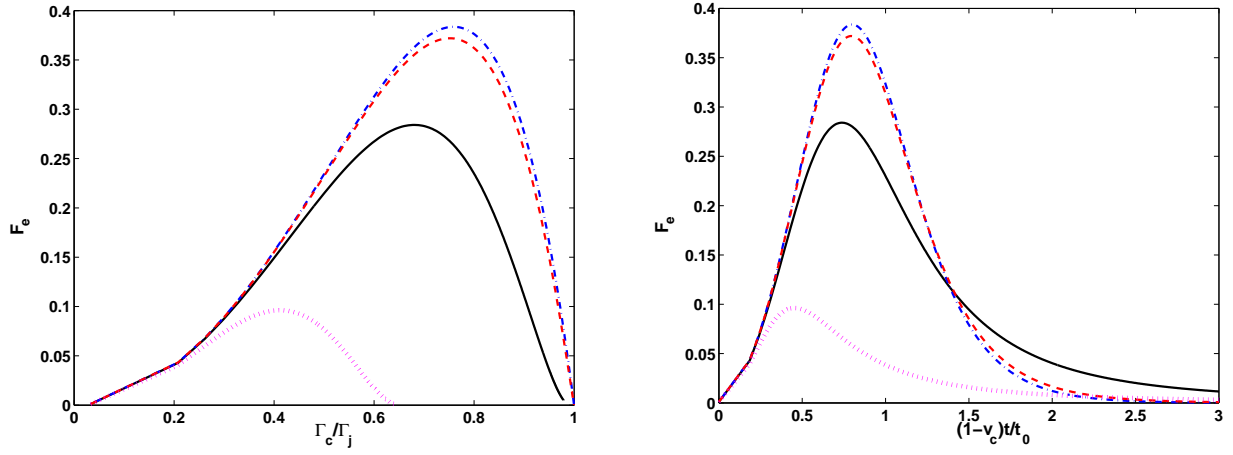


FIG. 2.— Solutions of Equation (13) shown as F_e vs. the relative Lorentz factor of the cloud (left panel) and as F_e vs. the observation time (in units $t_0 = z_0/2D\Gamma_j^2 c$) (right panel). The Lorentz factor of the jet is assumed to be $\Gamma_j = 30$. The following values of the D -parameter were used: $D = 100$ (dot-dashed lines), $D = 10$ (dashed line), $D = 1$ (solid line) and $D = 0.1$ (dotted line).

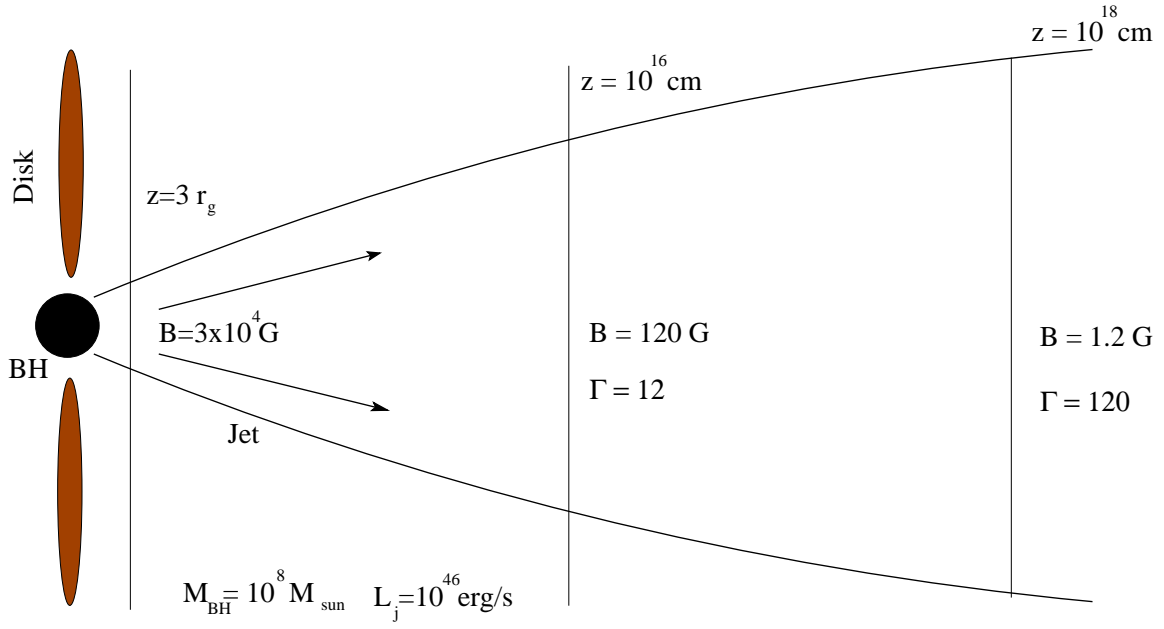


FIG. 3.— Sketch of the jet together with characteristic magnetic field strength and bulk Lorentz factors at typical distances from the BH. The BH mass and the dimensionless parameter of rotation were assumed to be $M_{\text{BH}} = 10^8 M_{\odot}$ and $a \approx 1$, respectively. Initially, the jet is assumed to be magnetically dominated with the magnetization parameter $\sigma \gtrsim 100$.

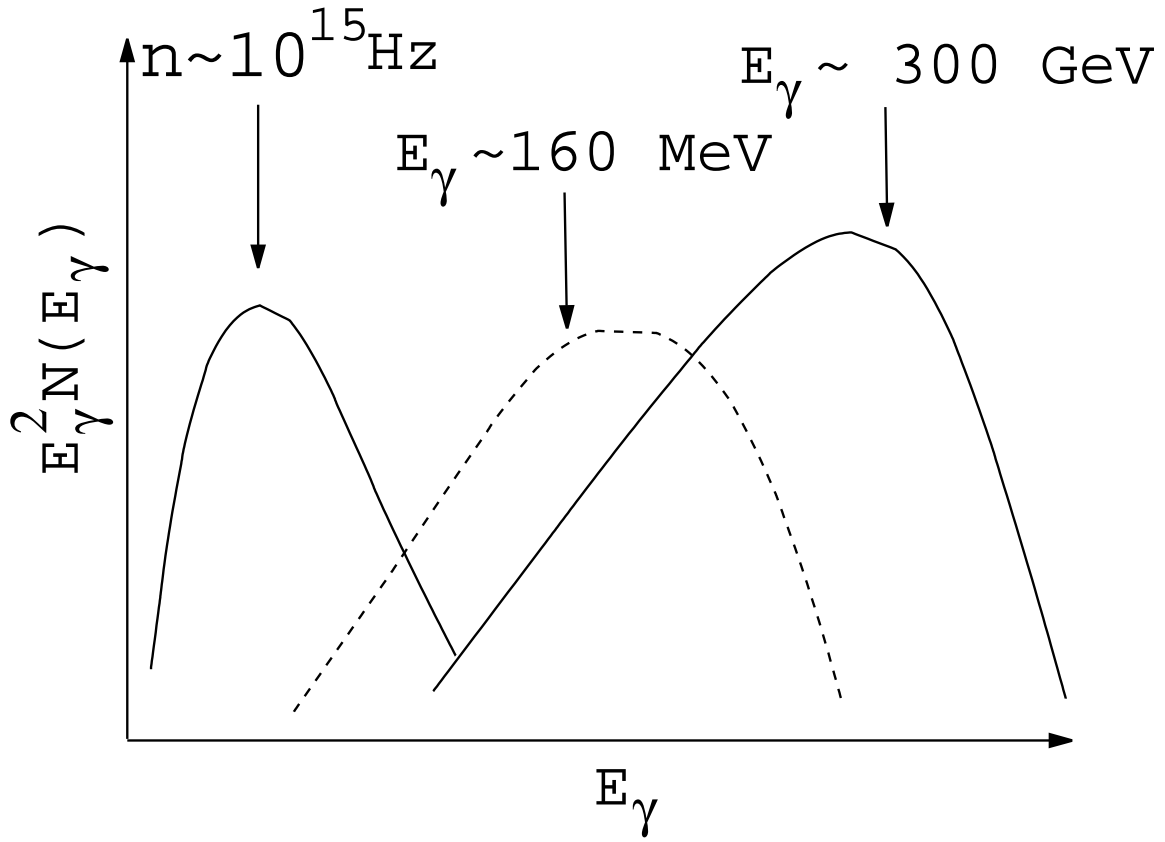


FIG. 4.— Expected SED of blazars in the framework of the proton-synchrotron scenario in the blob's reference frame. The maximum at 10^{15} Hz is due to synchrotron radiation from secondary (pair-produced) electrons; the maximum at $\sim 100 \text{ MeV}$ corresponds to the synchrotron radiation of primary electrons accelerated in the blob; the maximum at $\sim 300 \text{ GeV}$ is generated by protons through the synchrotron channel.

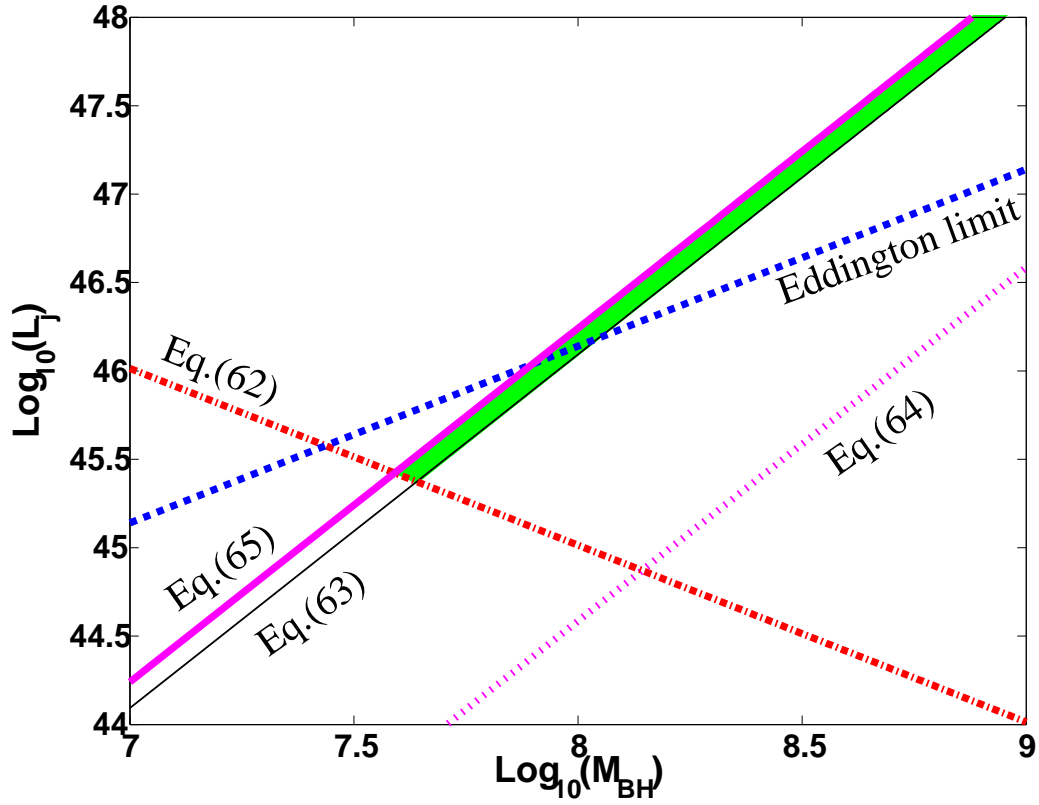


FIG. 5.— Intensive VHE flares (in the case EIC) of $L_\gamma \approx 10^{47} \text{ erg s}^{-1}$ and of duration $\tau \approx 200 \text{ s}$ that are energetically allowed in the framework of our JRGI scenario in systems characterized by a jet of luminosity, L_j , powered by a black hole of mass M_{BH} , are shown by the green filled region (we assume $\Gamma_j = 90$ and $\xi_{-1} = 1$). The thin solid line is the limit from Equation (63); the thick solid line is the limit from Equation (65); the dotted line is the limit from Equation (64); the dot-dashed line is the limit from Equation (62); and the dashed line is the Eddington limit.

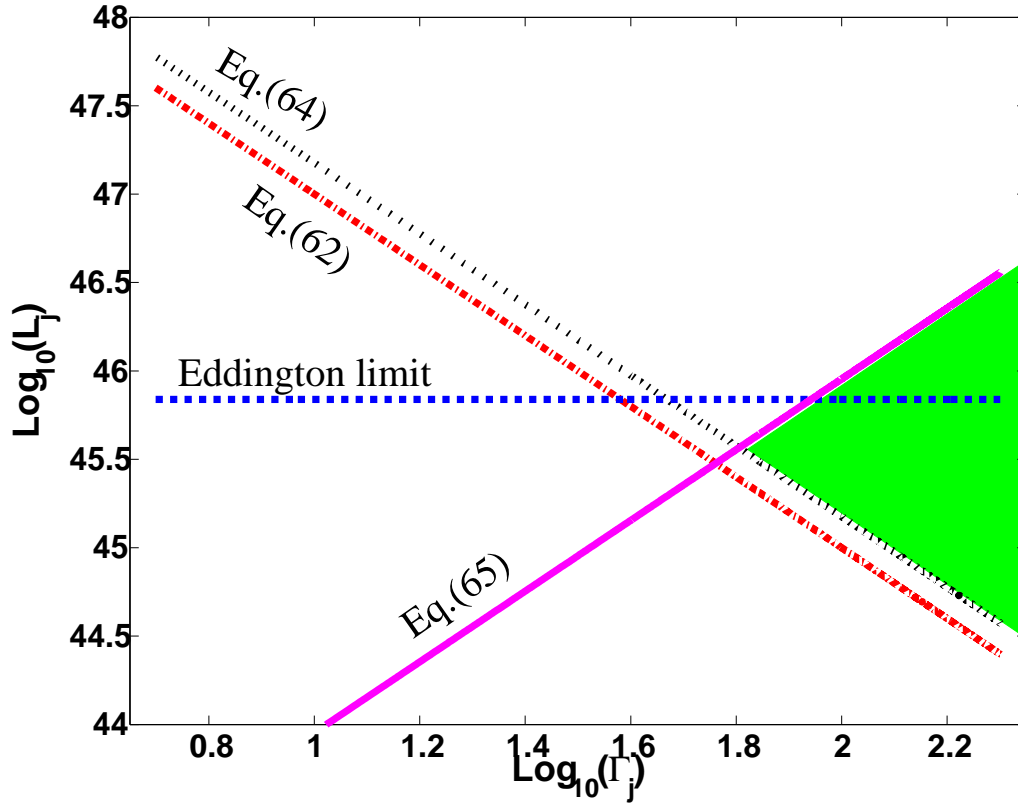


FIG. 6.— Intensive VHE flares (in the case EIC) of $L_\gamma \approx 10^{47} \text{ erg s}^{-1}$ and of duration $\tau \approx 200 \text{ s}$ that are energetically allowed in the framework of our JRGJ scenario in systems characterized by a jet of luminosity, L_j , propagating with bulk Lorentz factor Γ_j , are shown by the green filled region (here we assume $M_{\text{BH}} = 5 \times 10^7 M_\odot$ and $\xi_{-1} = 1$). The thin solid line is the limit from Equation (63); the thick solid line is the limit from Equation (65); the dotted line is the limit from Equation (64); the dot-dashed line is the limit from Equation (62); and the dashed line is the Eddington luminosity.

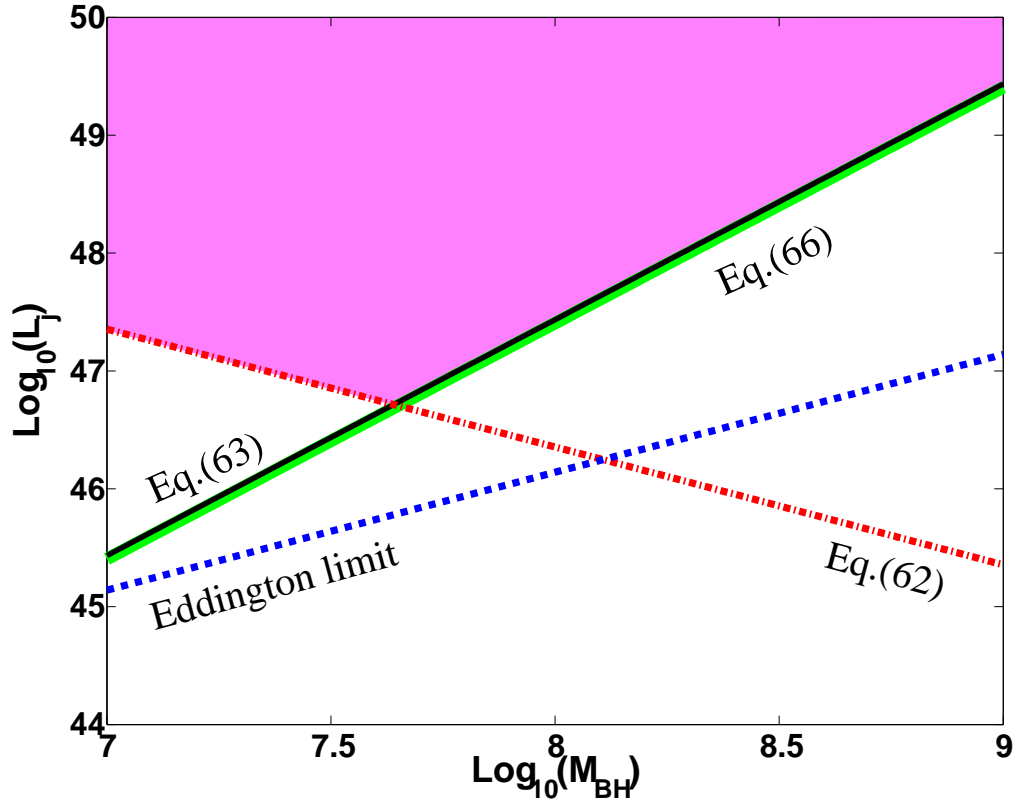


FIG. 7.— Intensive VHE flares (in the case of proton synchrotron) of $L_\gamma \approx 10^{47} \text{ erg s}^{-1}$ and of duration $\tau \approx 200 \text{ s}$ that are energetically allowed in the framework of the JRGI scenario in systems characterized by a jet of luminosity, L_j , powered by a black hole of mass M_{BH} , which are shown by the pink filled region (we assume $\Gamma_j = 20$ and $\xi_{-1} = 1$). The thin solid line is the limit from Equation (63); the thick solid line is the limit from Equation (66); the dot-dashed line is the limit from Equation (62); and the dashed line is the Eddington luminosity.

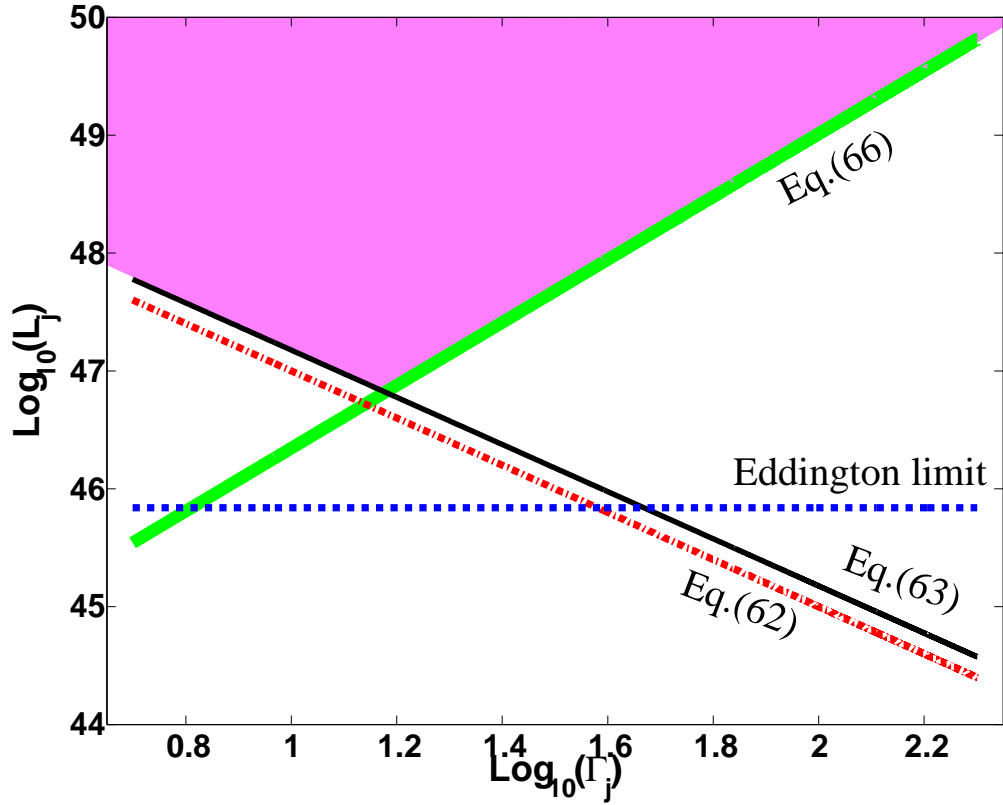


FIG. 8.— Intensive VHE flares (in the case of proton synchrotron) of $L_\gamma \approx 10^{47} \text{ erg s}^{-1}$ and of duration $\tau \approx 200 \text{ s}$ that are energetically allowed in the framework of the JRGI scenario in systems characterized by a jet of luminosity, L_j , propagating with bulk Lorentz factor Γ_j , are shown by the pink filled region (we assume $M_{\text{BH}} = 5 \times 10^7 M_\odot$ and $\xi_{-1} = 1$). The thin solid line is the limit from Equation (63); the thick solid line is the limit from Equation (66); the dot-dashed line is the limit from Equation (62); and the dashed line is the Eddington luminosity.

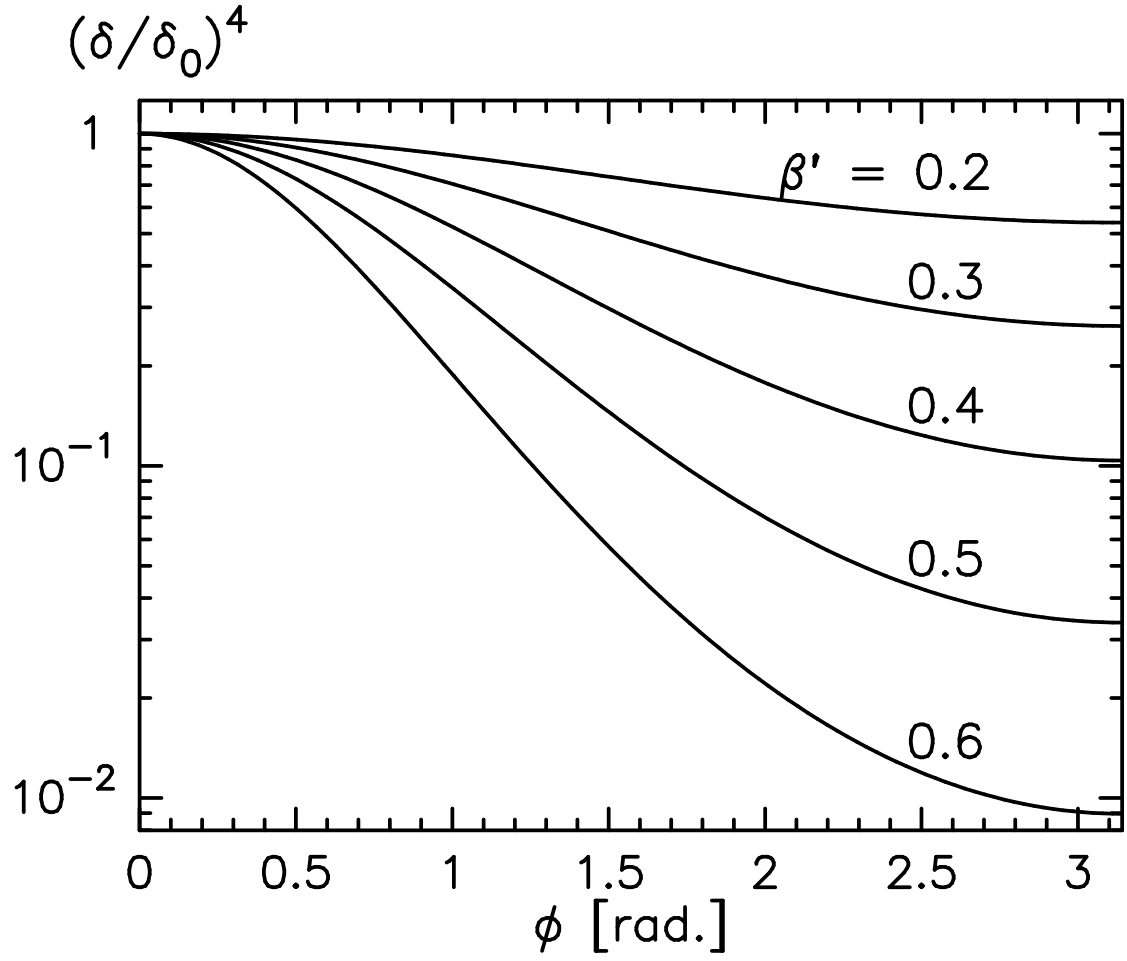


FIG. 9.— Dependence of the observed emission intensity, as defined by Equation (B9), on the position of the blob. The intensities are normalized to the maximum values (i.e the value at $\phi = 0$). The values of the parameter β' are shown in the figure.

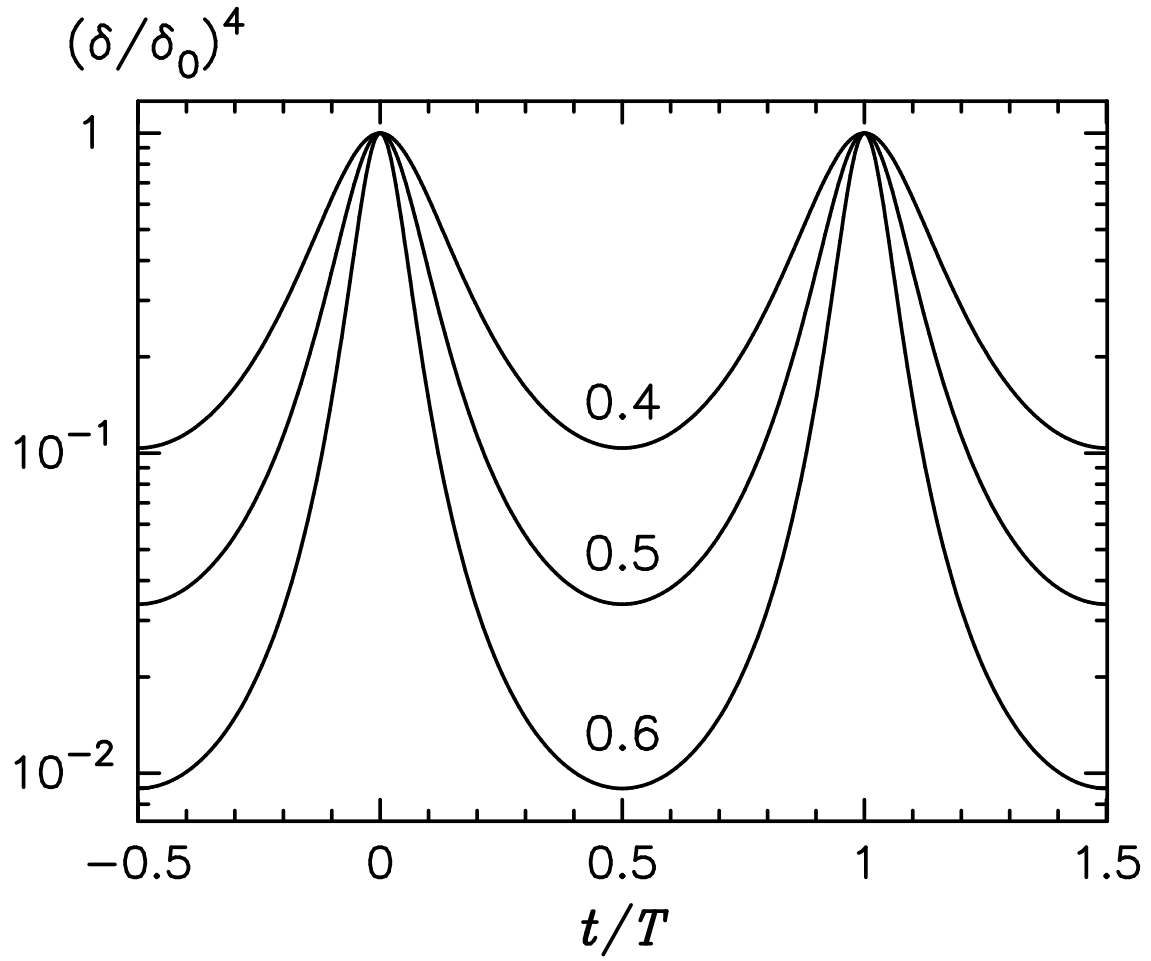


FIG. 10.— Dependence of the observed emission intensity (i.e. Equation (B9)) as a function of time, as obtained in Equation (B13), for three different values of the β' parameter: $\beta' = 0.4, 0.5$ and 0.6 (in the case B).

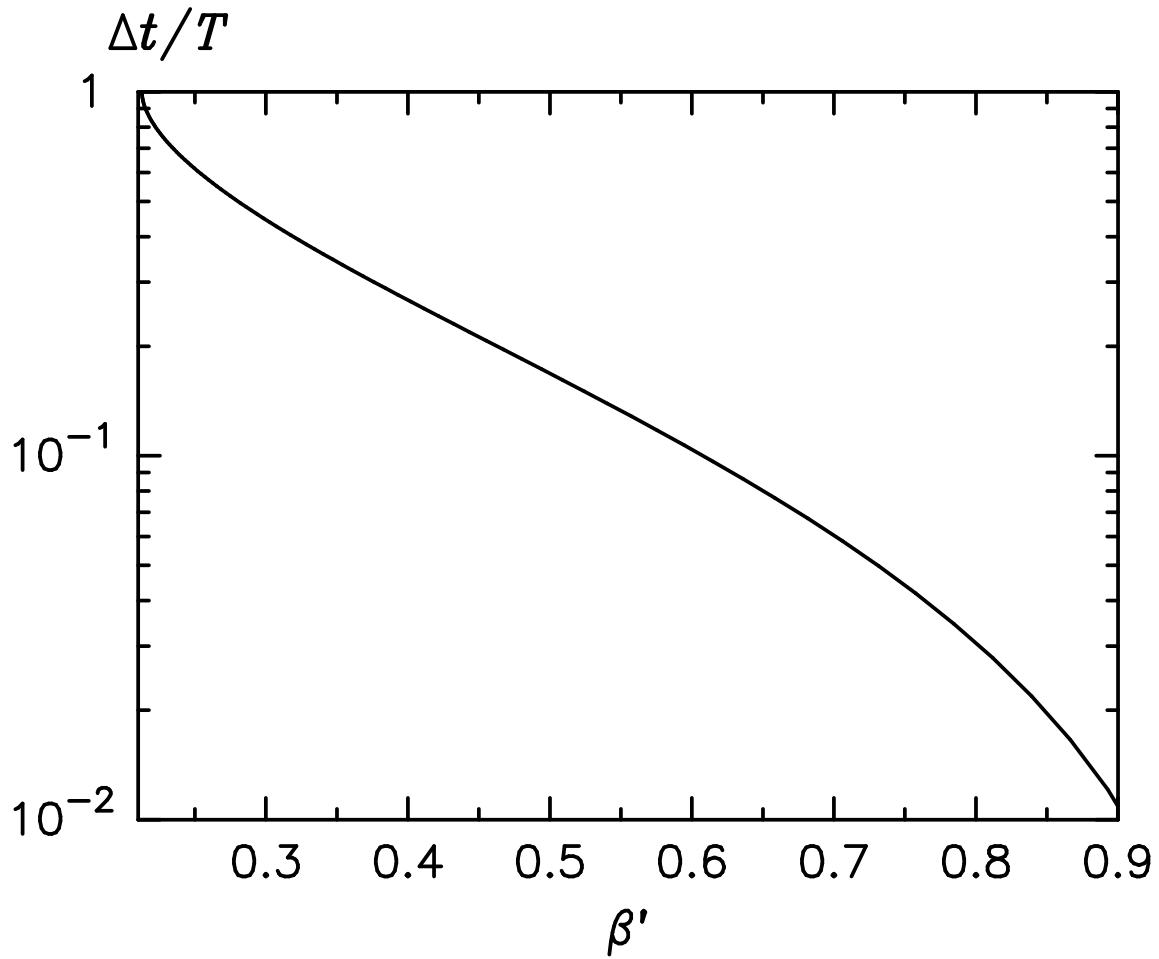


FIG. 11.— The width of the intensity peaks, shown in Figure 10, as function of β' (for details, see Appendix B, case B).